공학박사학위논문

Thermal behavior of surface films and its effect on electrochemical properties of graphite negative electrode for lithium-ion batteries

리튬 이온 전지용 흑연 음극에서 표면 필름의 열적 거동에 따른 전기화학 특성

2014년 2월

서울대학교 대학원

화학생물공학부

박 호 상

Abstract

The graphite negative electrode is now mainly employed in rechargeable lithium-ion batteries (LiBs). As its charge/discharge potential is beyond the electrochemical stability window of common non-aqueous organic electrolytes, the electrolytes are reductively decomposed in the charging (lithiation) period. Such electrolyte decomposition induces the formation of surface films on the negative electrode, often called solid electrolyte interphase (SEI). SEI layers on the graphite negative electrode play a critical role of determining the cell performances, which should satisfy the following requisites: mechanical stability, thermal stability, adhesion to electrode, insolubility and so on. Among them, the thermal stability of surface films is one of the most crucial criteria to affect the cell cycle life, calendar life, and even safety. In this study, the thermal behavior of SEI films and its effects on the electrochemical properties of graphite negative electrodes were investigated.

Firstly, the thermal stability of SEI derived from the standard electrolyte prepared by dissolving lithium hexafluorophosphate ($LiPF_6$) in ethylene carbonate/diethyl carbonate solvent is assessed using the open-circuit voltage (OCV) measurements. During a pre-cycling (a SEI formation step), reduction of ethylene carbonate (EC) was observed at 0.7 V (*vs.* Li/Li^+) in the first lithiation process; however, it disappeared in the sequent cycles. The OCV measurement with temperature ramp from 25^oC to 120^oC shows that the value of OCV increased dramatically up to 3.0 V (*vs.* Li/Li^+) above 60^oC. The OCV increase is consistent with loss of electrons in the graphite electrode,

which transferred to the interface between electrode and electrolyte because of the open-circuit system. Namely, it is concluded that the thermally damaged SEI layers lost its passivating ability (electron insulator). Identical behaviors were observed in the OCV measurement at a fixed temperature of 55 and 85^{o}C.

In the next part, the thermal behavior of surface films during high temperature storage at 85^{o}C and its effect on electrochemical properties are investigated. In the de-lithiated state (SOC0, state-of-charge), SEI films suffered thermal degradation more and more upon increase of storage time, which induces morphological and chemically compositional change in the surface films. The well-covered surface becomes rough by crumbling of films. In the chemical composition, high population of F-containing inorganic species, especially salt decomposed products appeared after high-temperature storage. And also, evidence of the surface exposure of graphite electrodes was observed from carbon 1s spectra. All these features caused to deteriorate the electrochemical properties, especially the Coulombic efficiency. On the contrary, the lithiated graphite negative electrodes (high SOC) show different thermal behavior and electrochemical performances. The value of OCV slightly increased; however, sufficient electrons were consumed to reform the thermally damaged surface films during the OCV increase. Such reformation of surface films was mainly derived from EC reductive decomposition, which is enriched by organic species with uniform coverage. The regenerated surface films during high-temperature storage play a good passivating ability as the original SEI layers does.

Finally, a comparative study on thermal stability of two SEI films on graphite

negative electrodes is conducted. The SEI films are generated by reductive decomposition of two different electrolyte solutions: that are the $LiPF_6$-based standard electrolyte and the controlling electrolyte prepared by dissolving lithium bis(trifluoromethylsulfonyl)imide (LiTFSI) in same carbonate solvent. The surface film generated from the standard electrolyte is thermally degraded with a substantial change in both film morphology and chemical composition to lose its passivating ability upon high-temperature exposure. The poorer thermal stability has been ascribed to a high population of Li- and F-containing inorganic species and presence of cracks or void spaces in the SEI layer. In contrast, the surface film derived from the controlling electrolyte, which is enriched by organic carbon-oxygen species with uniform coverage, remains rather intact in both chemical composition and film morphology after 85^{o}C-temperature storage, indicative of a superior thermal stability. As a result, this SEI layer maintains its passivating ability even after high-temperature storage.

Keywords: Lithium-ion batteries, Graphite, Solid electrolyte interphase (SEI), Thermal stability, Passivating ability

Student number: 2008-21080

List of Figures

Fig. 7. The irreversible capacity and the Coulombic efficiency of Li/MCMB cells before and after high-temperature storage at (a) 55^{o}C and (b) 85^{o}C.

Fig. 8. Differential capacity (dQ/dV) plots obtained in the initial two lithiation periods and after high-temperature storage at (a) 55^{o}C and (b) 85^{o}C for 24 h. The galvanostatic charge/discharge was performed at 25^{o}C, from which the dQ/dV profiles were derived.

Fig. 9. The variation of open-circuit voltage (OCV) of the Li/MCMB cell during high-temperature storage at 85^{o}C for 24 h. (i) C region and (ii) T region.

Fig. 10. The irreversible capacity and the Coulombic efficiency of Li/MCMB cells after high-temperature at 85^{o}C storage for 0 (before storage), 1, and 2 h.

Fig. 11. (a) The galvanostatic charge/discharge voltage profiles of the Li/MCMB cells obtained at 25^{o}C in the first cycle and after high-temperature storage at 85^{o}C. Specific current = 37.2 mA g^{-1}. Voltage cut-off range: 0.001~2 V. (b) Differential capacity (dQ/dV) plots derived from the above voltage profiles.

Fig. 12. FE-SEM images taken on the surface MCMB electrodes: (a) pristine, (b) before storage (after a pre-cycling), and after high-temperature storage at 85^{o}C for (c) 1 h, and (d) 2 h.

Fig. 13. C 1s XPS spectra obtained from the MCMB electrodes: (a) pristine, (b) before storage (after a pre-cycling), and after high-temperature storage at 85^{o}C for (c) 1 h, and (d) 2 h.

Fig. 14. (a) O 1s and (b) F 1s XPS spectra obtained from the MCMB electrodes before storage (after a pre-cycling) and after high-temperature storage at 85^{o}C for 1 and 2 h.

Fig. 15. The galvanostatic charge (lithiation) voltage profile of the Li/MCMB cell obtained at 25^{o}C. Specific current = 37.2 mA g^{-1}. Marks on the SOC0, SOC25, SOC50, SOC75, and SOC100 (in here, SOC100 = 300 mA h g^{-1}).

Fig. 16. The variation of open-circuit voltage (OCV) of the Li/MCMB cell during high-temperature storage at 85^{o}C.

Fig. 17. XRD patterns obtained from the MCMB electrodes before (bold solid lines) and after (thin solid line) high-temperature storage at 85^{o}C for 24 h.

Fig. 18. (a) The galvanostatic intermittent titration technique (GITT) voltage profile obtained with the Li/MCMB cell after a pre-cycling. (b) closed-circuit voltage (CCV) and quasi-open-circuit voltage (QOCV) profiles derived from the above-

represented GITT voltage profile.

Fig. 19. The OCV variation on the quasi-open-circuit voltage (QOCV) profile before (circle) and after (empty circle) high-temperature storage at 85^{o}C for 24 h.

Fig. 20. The galvanostatic charge/discharge voltage profiles of Li/MCMB cells before (dash line) and after (solid line) high-temperature storage at 85^{o}C for 24 h.

Fig. 21. The variation of open-circuit voltage (OCV) of Li/MCMB cells during high-temperature storage at 85^{o}C for 24 h. Marks on 12 h and 24 h-storage time for SOC0, SOC25, and SOC100.

Fig. 22. The irreversible capacity and the Coulombic efficiency of Li/MCMB cells after high-temperature at 85^{o}C storage for 12 h and 24 h.

Fig. 23. The galvanostatic charge/discharge voltage profiles of Li/MCMB cells obtained at 25^{o}C after high-temperature storage at 85^{o}C for 12 h (dash line) and 24 h (solid line). Specific current = 37.2 mA g^{-1}. Voltage cut-off range: 0.001~2 V.

Fig. 24. Differential capacity (dQ/dV) plots obtained after storage at 85^{o}C for 12 h and 24 h. The galvanostatic charge/discharge was performed at 25^{o}C, from which the

Specific current = 37.2 mA g^{-1}. Voltage cut-off range: 0.001~2 V. (b) Differential capacity (dQ/dV) plots derived from the above-represented voltage profiles.

Fig. 32. The Coulombic efficiency of Li/MCMB cells using either $LiPF_6$ or LiTFSI-based electrolyte before and after high-temperature storage at 85°C.

Fig. 33. The galvanostatic charge/discharge voltage profiles of the Li/MCMB cells using either $LiPF_6$ or LiTFSI-based electrolyte, which are obtained at 25°C in the initial two cycles and after high-temperature storage at 85°C for 24 h. Specific current = 37.2 mA g^{-1}. Voltage cut-off range: 0.001~2 V.

Fig. 34. Differential capacity (dQ/dV) plots obtained in the initial two lithiation periods and after high-temperature storage at 85°C for 24 h. The galvanostatic charge/discharge was performed at 25°C, from which the dQ/dV profiles were derived: (a) in the $LiPF_6$ and (b) the LiTFSI-based electrolyte.

Fig. 35. The variation of open-circuit voltage (OCV) of the Li/MCMB cells using either $LiPF_6$ or LiTFSI-based electrolyte during high-temperature storage with a temperature sweep from 25°C to 120°C at a ramp rate of 0.1°C min^{-1}.

Fig. 36. The variation of open-circuit voltage (OCV) of the Li/MCMB cells using either $LiPF_6$ or LiTFSI-based electrolyte during high-temperature storage fixed

the LiTFSI-based electrolyte before (dash line) and after (solid line) high-temperature storage at 85^{o}C for 24 h.

Fig. 43. Consumed capacity of Li/MCMB cells cells using either $LiPF_6$ or LiTFSI-based electrolyte during high-temperature storage at 85^{o}C for 24h.

Fig. 44. Differential capacity (dQ/dV) plots of the Li/MCMB cells using LiTFSI-based electrolyte in the first lithiation period and after high-temperature storage at 85^{o}C for 24 h. The galvanostatic charge/discharge was performed at 25^{o}C, from which the dQ/dV profiles were derived.

List of Tables

Contents

1. Introduction

The market of rechargeable lithium-ion batteries (LiBs) have been expanded since Sony released the first commercial LiBs in 1991. LiB is advantageous in terms of volumetric and gravimetric energy density [1]. Thanks to its superior performances to other conventional batteries, LiB has so far been adopted as major power sources in various portable electronic devices such as mobile cellular phones, smart phones, laptops, and tablet PCs. It would not be an exaggeration to say that LiBs has contributed to the development of IT (Information Technology). Even further, the application of LiBs has been expanded to power sources for hybrid electric vehicles (HEV) and electric vehicles (EV). It is also considered as one of the most promising candidates for energy storage system (ESS) and smart grid system. Namely, the market and application of LiBs is being enlarged from small to medium/large-size systems. For these applications, the following characterizations of LiBs should be required: high energy density, high power density, long cycle life, safety, and low cost. Especially, the temperature characterization is regarded as a crucial requisite because of the frequent exposure to exterior environment.

LiBs consist of main four components: anode (negative electrode), cathode (positive electrode), electrolyte, and separator. The conventional LiBs have used graphite and lithium cobalt (III) oxide ($LiCoO_2$) as anode and cathode, respectively. The electrolyte solution is prepared by dissolving lithium hexafluorophosphate ($LiPF_6$) in a mixture of cyclic carbonate and linear carbonate solvents. The separator is a polymeric membrane

with microporous layers such as poly propylene (PP) and poly ethylene (PE). The working potential of the graphite negative electrodes is close to that of lithium metal [2-5]. As its charge/discharge potential is beyond the electrochemical stability window of common non-aqueous carbonate-based electrolytes, the electrolytes are reductively decomposed upon contact (for Li metal) or in the charging (lithiation) period (for graphite) [6-9]. The electrolyte decomposition is not desirable for graphite negative electrodes because an extra amount of positive electrode materials should be loaded to compensate the electric charges/Li^+ ions consumed for the reductive electrolyte decomposition. Nonetheless, the electrolyte decomposition is beneficial in the other sense since a surface film forms on the negative electrode [8,10]. Such surface films, often called solid electrolyte interphase (SEI), are Li^+ ion conducting such that they do not induce a concentration polarization for lithium reactions. Moreover, the SEI layers are electronically insulating, such that any electrochemical reactions are hindered at the electrode/electrolyte interface, once they deposit up to a certain thickness, due to a negligible electron tunneling through the layer. Due to this passivating effect, additional electrolyte decomposition and thickening of SEI layer are suppressed. The present lithium-ion batteries (LIBs) outperform the other secondary cells with respect to coulombic efficiency and cycle life, which is due to the passivating role of SEI layers [11].

For a safer and longer operation of LIBs, SEI layers should meet other requirements besides the Li^+ ion conducting and electronically insulating properties. They should uniformly cover the electrode surface. Otherwise, the current distribution for lithium

reactions is not uniform. In general, thinner SEI is favored to minimize the ohmic resistance as far as it acts the passivation role. And also, their strong adhesion to electrode and physicochemical stability are required. Thermal stability must be another important requirement since SEI layers are vulnerable to damage upon a high-temperature exposure. Taking into account the fact that SEI films comprise a variety of inorganic or organic ingredients with a wide distribution in molecular weight, one can readily assume thermal instability of surface films. Some ingredients may be thermally decomposed and the other may be dissolved [12-15]. Once thermally degraded, the SEI layer will lose its passivating ability to cause additional electrolyte decomposition, which eventually leads to a self-discharge, poor cycleability, and other undesirable features for LIBs [12,13,15-20]. Moreover, thermal instability can pose a serious safety concern since the damage of SEI can trigger a thermal runaway, in which cell temperature increases uncontrollably due to successive exothermic reactions [21,22]. Several previous papers reported the instability of SEI layers and their degradation mechanisms at elevated temperatures [12,13,15,17,23-26]. Thermal decomposition of a meta-stable ingredient such as lithium alkyl carbonates ($ROCO_2Li$) to a stable product has been proposed [23,24]. The changes in film morphology and chemical compositions upon high-temperature exposure have also been reported in several papers [12,13,17,20,24]. Obviously, thermal properties of SEI layers are strongly associated with the ingredients of SEI, thickness, and morphology. All these features are in turn dictated by the electrolyte components (organic solvent and lithium salt) in addition to the working conditions [24,27-29].

In this work, the thermal stability of SEI derived from conventional $LiPF_6$-based electrolyte is evaluated by means of the electrochemical analyses. The primary objective is to address useful electrochemical analysis to assess thermal stability of surface films. Secondly, the thermal behavior of surface films during high-temperature storage is elucidated. For this goal, variables of SOC (state-of-charge) and storage time were controlled. And also, the effect of thermal behavior on the electrochemical properties in the graphite negative electrode is investigated. Lastly, the improvement for thermal stability of films is proposed in a viewpoint of lithium salts. Thermal stability is compared for two SEI films that are generated from two different electrolytes with either $LiPF_6$ or LiTFSI (lithium bis(trifluoromethylsulfonyl)imide). It is proposed to address how chemical composition and film morphology have an effect on thermal stability of SEI films. X-ray photoelectron spectroscopy (XPS) and scanning electron microscope (SEM) were utilized to analyze the film composition and morphology, whereas an open-circuit voltage (OCV) measurement was performed at elevated temperatures to assess the thermal stability of SEI films.

2. Background

2.1. Electrochemistry and electrochemical cell

Electrochemistry is a branch of chemistry that studies electrochemical reactions. The electrochemical reactions involving electrons are divided into two reactions; oxidation and reduction reaction. Oxidation is the loss of electrons, and reduction is the gain of electrons.

$$\mathrm{R} \rightarrow \mathrm{O} + ne \text{ (oxidation)}$$

$$\mathrm{O} + ne \rightarrow \mathrm{R} \text{ (reduction)}$$

In the electrochemical reactions, charge transfer where electrons are transferred between electrodes and reactants should take place and electrons are transferred by means of quantum tunneling. Generally, the tunneling rate exponentially decreases with the increase of tunneling length; therefore, the charge transfer is restrictively possible between electrodes and reactants which are very close to the electrodes.

The electrochemical cell is a device capable of converting the chemical energy of active materials into the electrochemical energy through electrochemical redox reactions. Generally, a cell is a unit of basic electrochemical cells and a battery consists of more than two cells by a series or a parallel. The electrochemical cell should require

three main components; anode, cathode and electrolyte. Anode is an electrode with oxidation reaction, and cathode with reduction reaction. In the electrochemical cell, the system should form “closed loop” in which electrochemical redox reactions always happen simultaneously (Fig. 1).

$$aA \rightarrow cC + ne \text{ (oxidation in anode)}$$

$$bB + ne \rightarrow dD \text{ (reduction in cathode)}$$

- A, B, C, D is reactants
- *a*, *b*, *c*, *d* is moles of reactants participating in electrochemical reactions
- *n* is moles of electrons participating in electrochemical reactions

The total reaction is represented by the sum of the electrochemical reaction in each half cell.

$$aA + bB \rightarrow cC + dD \text{ (the total reaction)}$$

The standard Gibbs free energy (ΔG^o) of this total reaction is:

$$\Delta G^o = -nFE^o$$

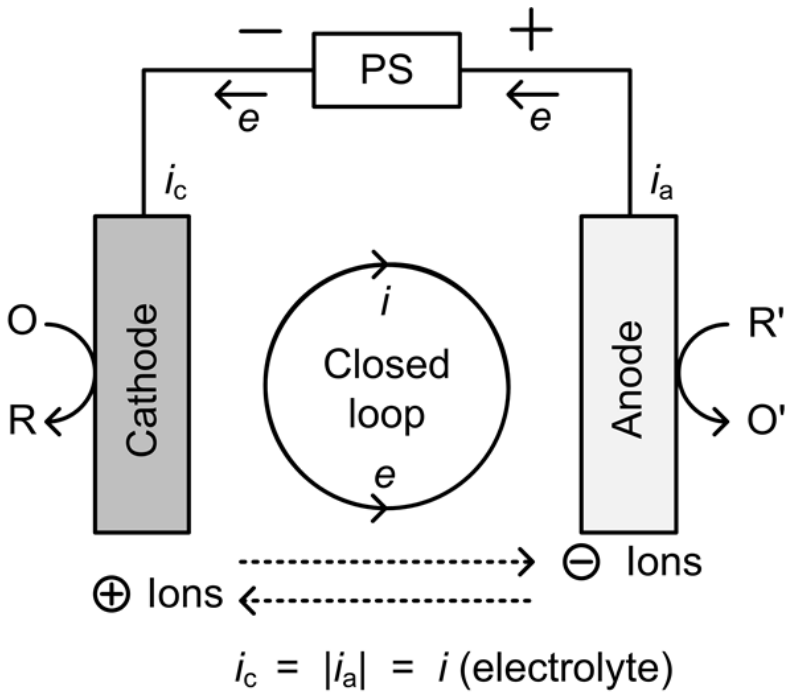

Figure 1. The closed loop in the electrochemical cell consisting of anode, cathode, electrolyte, and power supply.

- F is the Faraday constant, $9.6485 \times 10^4\ C\ equiv^{-1}$
- E^o is a standard electrode potential (V)

At standard condition, when the standard Gibbs free energy is positive ($\Delta G^o > 0$), the total reaction is not spontaneous. The system (electrolytic cells) needs external electrochemical energy to induce the electrochemical reactions. On the contrary, when the standard Gibbs free energy is negative ($\Delta G^o < 0$), the total reaction is spontaneous to get the electrochemical energy in the system (galvanic cells). The electromotive force (emf) can be calculated from the standard Gibbs free energy change in the total reaction. In non-standard conditions, the equilibrium potential (E_{eq}) is derived from Nernst equation.

$$E_{eq} = E^o + \frac{RT}{nF} \ln \frac{a_A^a \cdot a_B^b}{a_C^c \cdot a_D^d}$$

- a_i is an activity of substance *i*
- R is a gas constant, $8.314\ J\ K^{-1}\ mol^{-1}$
- T is an absolute temperature (K)

2.2. Lithium-ion batteries

Lithium is the lightest metal belonging to the alkali group. Its standard reduction

potential is the lowest, -3.045 V (*vs.* NHE). Owing to these features, lithium has been paid attention to as the electrode material with high energy density. Lithium metal, however, is highly reactive and vigorously reacts with water in the aqueous system. Generally, the system using lithium as an electrode material employs organic or inorganic non-aqueous electrolytes, where lithium can react with non-aqueous electrolytes chemically or electrochemically. Nonetheless, lithium can be available for electrochemical cell systems since passivation films formed at the surface of lithium metal plays a role of suppressing additional side reactions [10,30].

The lithium-ion battery (LiB) is a type of rechargeable batteries in which lithium ions move between anode (negative electrode) and cathode (positive electrode) during charge/discharge process. In 1970s, The rechargeable LiBs were first proposed by M. S. Whittingham [31]. The cell consisted of lithium metal and titanium (IV) sulfide (TiS_2) as negative and positive electrode, respectively. The systems using metallic lithium as negative electrode had ceaseless problems since the primary lithium batteries. Safety issue was one of the critical drawbacks. The charge/discharge process provoked to generate lithium dendrite on the surface of metallic lithium electrode. This lithium dendrite could penetrate a separator and contact to positive electrode, which induced “internal short” in the cell and the cell might even explode by thermal runaway. To improve the drawbacks of lithium metal, many researchers made efforts to apply the materials capable of reversible insertion of lithium ions. In 1974, reversible intercalation/de-intercalation of NR_4^+ ion in graphite was discovered by J. O. Besenhard [32]. He proposed its application of graphite to LiBs [33,34]. Replacement

of lithium metal by lithium-ion insertion materials improved both cycle life and safety.

Meanwhile, replacement of metallic lithium in the negative electrode motivated the development of lithium ion-containing positive electrode materials; because there was no lithium-ion sources except lithium salts in the electrolyte. J. B. Goodenough first proposed the application of lithium cobalt (III) oxide ($LiCoO_2$) to LiBs in 1980s [35,36]. A combination of lithium-ion insertion negative electrode materials with lithium-ion insertion positive electrode materials gave birth of brand new concept of LiBs. Namely, one of the electrode materials releases lithium ion, which is inserted into the other electrode material [37]. This principle of lithium ion transfer was first proposed by M. B. Armand who named it “rocking chair” system (Fig. 2) [38]. In 1991, Sony released the first commercial LiBs in which carbonaceous materials and $LiCoO_2$ were used as negative and positive electrode materials, respectively.

2.3. Components in lithium-ion batteries

2.3.1. Negative electrode materials

In the early stage, lithium rechargeable batteries used lithium metal as a negative electrode material. The theoretical specific capacity of Li metal is about 3800 mA h g^{-1}; however, its low melting point and poor reversibility stunted the development of battery markets. Especially, the lithium dendrites formed during charge/discharge process provoke the internal short. The application of carbonaceous materials where

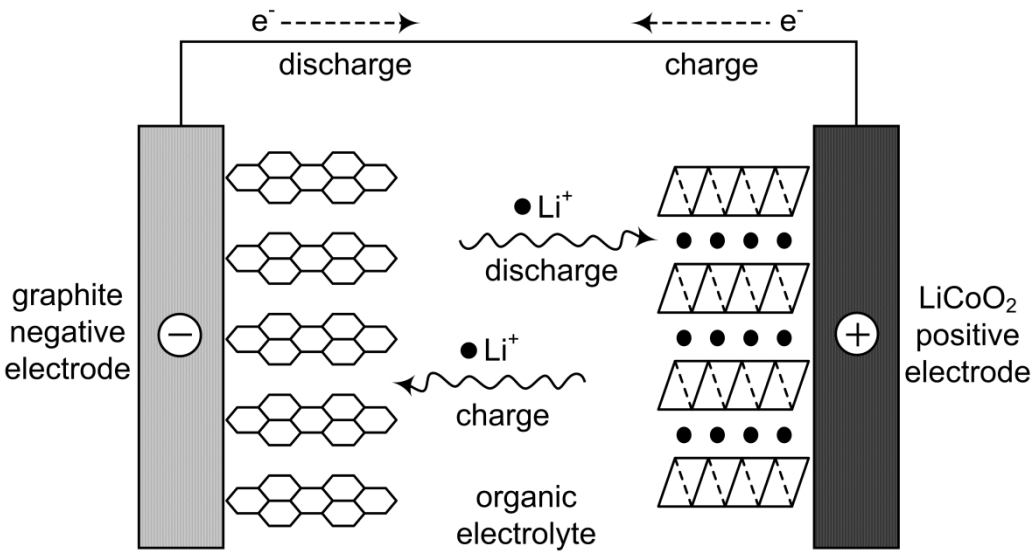

Figure 2. "Rocking chair" system in the lithium-ion batteries.

insertion of lithium ions is possible can handle the safety issues of lithium metal successfully. Moreover, carbonaceous materials have low working potential as much as lithium metal, good structural stability, and good cycleability. Among the carbonaceous materials, graphite is one of the most popular negative electrode materials and its theoretical specific capacity is 372 mA h g^{-1}. To overcome the limits of intrinsic capacity of graphite, alloy-based materials such as Si- and Sn-based materials have been developed. One of the demerits for alloy materials, however, is large volume expansion/shrinkage during alloying/de-alloying process, which causes pulverization of active materials, loss of electrical contact, and poor cycleability. These drawbacks of lithium alloy-based materials should be improved for commercialization.

2.3.1.1. Carbonaceous materials

Carbonaceous materials are divided into graphite and non-graphitic carbon (hard and soft carbon). Graphite has been most widely used in the LiBs. The theoretical specific capacity of graphite is 372 mA h g^{-1} (LiC_6) and lithium ions are stored in the graphitic interlayer through “intercalation” reaction [39]. Such an intercalation of lithium ions is conducted by solid-state diffusion. Therefore, its electrochemical reaction rate is rather slower than surface reaction derived from liquid-phase diffusion or electric double layer charging reaction for EDLC. Crystalline graphite has basal plane (perpendicular to c-axis) and edge plane (parallel to c-axis). Such an anisotropy of graphite affects the electrochemical reaction at each plane; relatively inactive in the basal plane and

vigorously active in the edge plane. Namely, lithium ions are intercalated mainly at the edge plane and possibly at defects of the basal plane. Lithium-ion intercalation reaction occurs under 0.3 V (*vs.* Li/Li^+), and intercalated lithium ions forms Li_xC compounds during lithiation process. When the concentration of intercalated lithium ions is low, lithium ions never intercalate in the neighboring graphitic layers but forms the layers by themselves. Such an arrangement of lithium-ion layers and graphitic layers is periodic. As the concentration of intercalated lithium ions gets higher and reaches the maximum value of LiC_6, lithium-ion layers and graphitic layers become arranged by turns. Such a lithium-ion intercalation process is called “staging” [40,41].

Non-graphitic carbon is categorized into hard (non-graphitizable) and soft (graphitizable) carbon [42]. Hard carbon is synthesized by carbonization of thermosetting resin or organic compounds, so it consists of three-dimensionally disordered cross-linked graphitic layers. Owing to such a disordered structure, hard carbon is hardly graphitized under the heat treatment over 2500^{o}C. On the contrary, graphitic layers of soft carbon are relatively arranged in parallel, so the heat treatment over 2500^{o}C enables its graphitization of soft carbon. Structural difference between graphite and non-graphitic carbon induces different reaction mechanism. For non-graphitic carbon, the intercalation reaction of lithium ions rarely occurs owing to the small size of crystallite consisting of graphitic layers. Nevertheless, non-graphitic carbon has lots of micro pores that can store lithium ions by means of adsorption or formation of clusters [43,44].

2.3.1.2. Lithium alloy-based materials

For substituting the conventional graphite negative electrode materials and enhancing the cell capacity in the LiBs, lithium alloy-based materials (Al, Si, Sn, Pb, In, Bi, Sb, and Ag) have been researched [45-47]. Typical lithium alloy-based negative electrode materials are Sn- and Si-based compounds. Such alloy-based materials react with lithium to form alloy during charging (lithiation for graphite) process and turns back to be metal during discharging (de-lithiation for graphite) process. Alloying/de-alloying process is quite reversible, so the application of alloy-based materials to LiBs has been considered optimistically. Lithium-metal alloy compounds can deliver much higher capacity than graphite (372 mA h g^{-1} for LiC_6). For Sn-based compounds, pure Sn reacts with Li to form alloy compounds of $Li_{22}Sn_5$ which can deliver the specific capacity of 900 mA h g^{-1}. Similarly, pure Si can turn to be $Li_{15}Si_4$ (3580 mA h g^{-1} at RT) and $Li_{21}Si_5$ (4008 mA h g^{-1} at elevated temperature) alloy phase during alloying process [48]. However, the intrinsic problem has hindered the commercialization of alloy-based materials. During alloying/de-alloying process, they suffer from large volume expansion/shrinkage and its volume change is from 100% to 400% [49]. Therefore, such huge volume change can provokes the pulverization of active materials, which induces loss of electrical contact. To solve this problem, various approaches have been presented: particulate, multi components-based complex, thin-film fabrication, and improvement of electrolyte additive [49-51].

2.3.2. Positive electrode materials

Among the components in LiBs, the positive electrode materials play a critical role of determining the cell capacity and performance. Layered $LiCoO_2$ has been used as the positive electrode material since Sony commercialized the LiBs in 1991. Layered $LiCoO_2$ has high working potential, good lithium ion diffusivity, and reasonably high capacity. As the needs for the high energy density and power density were required in LiBs, the researches for new positive electrode materials have been conducted. Layered $LiNO_2$, one of the high-capacity positive electrode materials, can deliver the higher capacity than Layered $LiCoO_2$; however, its structural instability during charge/discharge process causes the cell safety and it still remains a problem to be solved. The merits for the structural stability and low price can highlight spinel $LiMn_2O_4$, a spinel-structure compound, even though its lower capacity. Thanks to its spinel structure, good stability in the charged state improves the cell safety. Spinel $LiMn_2O_4$, however, can hardly overcome the limits of intrinsic capacity and it has been revealed that cell performance in the high temperature is a disaster because of manganese dissolution. Recently, olivine $LiFePO_4$, an olivine-structure compound, receives attention owing to high structural stability. Although lower conductivity and average working potential than conventional positive electrode materials, unique safety performance is fascinating.

2.3.2.1. Layered structure materials

Lithium transition metal oxides ($LiMO_2$) having a layered structure have been extensively studies as the positive electrode materials in the LiBs. Among those metal oxides, layered lithium cobalt oxide, $LiCoO_2$ has been considered a material with favorable electrochemical performances, and it has been most widely used as the positive electrode materials in the LiBs since J. B. Goodenough discovered this compound in 1980 [35]. In the $LiCoO_2$ layered structure (space group: $R\bar{3}m$), the unit cell consists of layers of lithium atoms that lie between slabs of octahedral CoO_6. With the removal of lithium ions from layered $LiCoO_2$, non-stoichiometric $Li_{1-x}CoO_2$ ($0 < x < 1$) compounds are formed, and their crystallographic structure is dependent on the lithium contents [52,53]. Reversible intercalation/de-intercalation, however, is possible within only half of lithium contents since it is irreversibly converted into monoclinic structure when $x > 0.5$ in $Li_{1-x}CoO_2$ during charge process. Such an irreversible phase transition limits the reversible specific capacity to about 140 mA h g^{-1} (charged up to 4.3 V *vs.* Li/Li^+) compared to the theoretical specific capacity of 274 mA h g^{-1}. The volume of unit cell and lattice parameters in layered $LiCoO_2$ also changes with the lithium contents. With the removal of lithium ions from layered $Li_{1-x}CoO_2$ up to $x = 0.5$, the crystalline expands along the c-axis due to repulsion between oxygen atoms [54,55]. Over 4.3 V ($x > 0.5$ in $Li_{1-x}CoO_2$), Oxygen evolution can occur rather than Co oxidation, which induces to decrease the reversible capacity. Moreover, the vigorous oxygen evolution accompanied by structural collapse of layered $LiCoO_2$ in the elevated

temperature can introduce the cell safety issue [56].

Layered lithium nickel oxide, $LiNiO_2$ has attracted intense attention since its redox potential is about 0.25 V lower than that of layered $LiCoO_2$, which can be profitable for electrolyte oxidation problems [57]. Compared to layered $LiCoO_2$, layered $LiNiO_2$ is cheaper and less toxic, and it can deliver higher reversible capacity (possible more than 200 mA h g^{-1}). Since the structural change rarely occurs with the lithium contents of layered $LiNiO_2$, the electrochemical properties can be maintained even at higher potential. Nonetheless, some problems should be solved for commercialization of layered $LiNiO_2$: (i) complicated synthesis, (ii) cation mixing, and (iii) low thermal stability. To solve those problems, the partial substitution of Mn, Co and Al for Ni and coating of Al_2O_3 and ZrO_2 on the surface has been studied [58-60].

2.3.2.2. Spinel structure materials

Spinel lithium manganese oxide, $LiMn_2O_4$ has been paid attention as an alternative to layered $LiCoO_2$ [61,62]. Spinel $LiMn_2O_4$ has many desirable merits including high rate performance (3-D host network), low cost and toxicity (manganese), and facile preparation (solid-state reaction). In the $LiMn_2O_4$ spinel structure (space group: Fd3m), a cubic close-packed (ccp) array of oxygen atoms occupy the 32e position, Mn and Li atoms are located in the 16d and 8a site, respectively. The Mn atoms have an octahedral coordination to the oxygen atoms, and the octahedral MnO_6 share edges in a three-dimensional host for the Li guest ions. During charge process, the unit cell

volume decreased gradually and isotropically as the concentration of lithium ions decreased. The removal of lithium ions from the spinel $LiMn_2O_4$ occurs through a two-step reaction at around 4.0 V (*vs.* Li/Li^+) where two voltage plateaus can be observed. Although the theoretical specific capacity of spinel $LiMn_2O_4$, about 150 mA h g^{-1}, is lower than that of layered $LiCoO_2$, the 3-D host network functions well in the 4V region. However, there are some problems that lead to cell degradation: (i) loss of Mn through disproportionation of trivalent Mn, (ii) Jahn-Teller distortion during charge/discharge process, and (iii) dissolution of divalent Mn caused by HF attack at elevated temperature [63,64]. To solve those problems, cation substitution (such as Al^{3+}, Ni^{3+}, Co^{3+}, and Fe^{3+}) has been proposed [65,66]. Solid solutions in which monovalent, divalent, or trivalent cations substitute the Mn cation to increase the average Mn oxidation state. Also, the attempts have been made to fabricate the protective surface coating with Al_2O_3, $AlPO_4$, ZrO_2, and ITO, which improve the stability of spinel $LiMn_2O_4$ and cycle performance at elevated temperature [67-69].

2.3.2.3. Olivine structure materials

Olivine lithium iron phosphate, $LiFePO_4$ has been recently highlighted owing to its superior structural stability and high specific capacity of about 170 mA h g^{-1} [70]. In the $LiFePO_4$ olivine structure (space group: Pnma), oxygen atoms arrange in terms of a hexagonal close-packed (hcp) structure, and the Fe atoms have an octahedral coordination to the oxygen atoms. The octahedral FeO_6 contacts with tetrahedral PO_4

by sharing oxygen vertices and links another tetrahedral PO_4 by sharing an edge. Lithium atoms are situated in the interstitial voids of the framework. Among the Fe-based compounds, olivine $LiFePO_4$ lowers the Fe^{3+}/Fe^{2+} redox energy to useful levels. Strong covalent bonding with the polyanion $(PO_4)^{3-}$ reduces the covalent bonding of Fe-O, which lowers the redox energy of Fe below the Fermi level of Li in olivine $LiFePO_4$. The Fe^{3+}/Fe^{2+} redox reaction in olivine $LiFePO_4$ occurs at around 3.4 V (*vs.* Li/Li^+) [70,71]. Although its structural and chemical stability is remarkably high, there are some demerits such as poor electrical conductivity (the general property of materials containing polyanion) and low lithium ion diffusivity (the 1-D host network of lithium insertion/extraction) [72,73]. To improve the electrical conductivity, coating with the conducting materials such as carbon and Ag nanoparticles and doping with heterogeneous atoms has been proposed. Also, the attempts to synthesize the nano-sized olivine $LiFePO_4$ particles have been made in order to improve the lithium ion diffusivity.

2.3.3. Electrolyte

In the electrolytes, lithium ions are solvated and the solvated lithium ions migrate from positive (or negative) electrode to opposite electrode during charge/discharge process. Namely, the electrolytes in the LiBs play a role of conveying the lithium ions smoothly and assisting the electrochemical reaction at the interface. Generally, electrolytes should satisfy the followings: (i) high ionic conductivity, (ii) high chemical

and mechanical stability, (iii) wide electrochemical stability windows, (iv) wide temperature ranges, and (v) low cost. The electrolytes used in the LiBs usually consist of organic solvents and lithium salts. The characteristics of the electrolytes are dependent on the each intrinsic property of organic solvents and lithium salts.

2.3.3.1. Organic solvents

The working potential of the LiBs is considerably high, so the usage of aqueous electrolytes is basically impossible but organic solvents, especially carbonate-based solvents, have been utilized for LiBs. Solvents should dissolve lithium salts well to obtain the high ionic conductivity and also have no reactivity with lithium ions. Therefore, aprotic solvents with high polarity are favorable. High ionic conductivity can be originated from the solvents having high dielectric constant and low viscosity. Generally, however, solvents with high dielectric constant have a tendency to raise the viscosity owing to the high polarity. Common approach is to mix cyclic carbonate (high dielectric constant) and linear carbonate (low viscosity). Ethylene carbonate (EC) and propylene carbonate (PC) in cyclic carbonates, and dimethyl carbonate (DMC), diethyl carbonate (DEC), and ethyl methyl carbonate (EMC) in linear carbonates are typical [74]. EC is most commonly used cyclic carbonate since it has reasonable properties such as high dielectric constant and good SEI former on the graphite electrode. Linear carbonates are used alone or together depending on the purpose.

2.3.3.2. Lithium salts

The role of lithium salts is to produce lithium ions and participate in migration of lithium ions in the electrolytes. Therefore, lithium salts should be dissolved well in organic solvents. Dissociation of lithium salts is strongly dependent on the properties of anions, especially large-sized. The tendency of dissociation in lithium salts is as follows: $Li(CF_3SO_2)_2N$ > $LiAsF_6$ > $LiPF_6$ > $LiClO_4$ > $LiBF_4$ > $LiCF_3SO_3$ [74,75]. On the other hand, lithium salts should be also considered in the other conditions such as non-toxicity, thermal and chemical stability, safety, tolerance for Al corrosion, and so on. Among the above-mentioned lithium salts, $LiPF_6$ is most appropriate lithium salt for the LiBs and has been used widely.

2.4. Solid electrolyte interphase (SEI)

Lithium metal is thermodynamically unstable toward the carbonate-based electrolytes. With a contact to electrolytes, metallic lithium is covered by a passivating film that enables the usage of lithium metal as the negative electrode in the lithium batteries. The spontaneous formation of a protective layer on metallic Li was discovered by E. Peled in 1979 [6]. The electrochemical reduction reaction on the graphite surface is similar to that on metallic lithium. During charge (lithiation) process, such a passivating film also forms on the graphite negative electrode in the LiBs [5]. The reaction potential of graphite is low enough to decompose the carbonate-based

electrolyte at the graphite surface. The organic and inorganic decomposed products deposited on the surface play a critical role of preventing additional electrolyte decomposition in the sequent cycles and thereby ensure good cycleability of the graphite negative electrode. The passivating films can kinetically protect the charged (lithiated) graphite that is thermodynamically unstable in the carbonate-based electrolytes. This essential passivating film is called “solid electrolyte interphase (SEI)” [6].

The onset potential of SEI formation on the graphite is 0.8 V (*vs.* Li/Li^+) for ethylene carbonate (EC)-based electrolytes [5]. Generally, SEI formation is not completed in the first cycle but continues up to few cycles, which depends on the several factors like cycling conditions (current density and temperature), nature of electrolytes and etc. A problem with the formation of a protective SEI film is that it consumes lithium ions and equivalent electrons. Namely, the formation of SEI is irreversible reaction with consequent loss of cell capacity. For the graphite electrode, the portion of irreversible capacity for SEI formation is less than 10% in the first charged capacity. So an extra amount of positive electrode materials should be loaded to compensate the irreversible capacity consumed for the SEI formation. As the electrolyte decomposition, namely SEI formation, is inevitable for the graphite electrode, lots of attempts have been made to form good SEI layers. The main approach is to use electrolyte additives (often called SEI forming agents) like vinylene carbonate (VC), fluoroethylene carbonate (FEC), and so on [76,77].

The fundamental properties of SEI layers are following: electrical insulator and

lithium ionic conductor. The SEI layers are Li^+ ion conducting such that they do not induce a concentration polarization for lithium reactions, and electronically insulating such that any electrochemical reactions are hindered at the electrode/electrolyte interface, once they deposit up to a certain thickness, due to a negligible electron tunneling through the layer. The SEI films on the graphite negative electrode play a critical role of determining the cell performances, which should satisfy the following requisites: mechanical stability, thermal stability, adhesion to electrode, insolubility and so on.

3. Experimental

3.1. Electrode preparation

To prepare graphite electrodes, a mixture of mesocarbon microbead (MCMB-10-28, average particle diameter = 10 μm, graphitization temperature = 2800^{o}C, Osaka Gas Co.) powder, Super P (a conductive carbon), and poly(vinylidene fluoride) (PVdF, KF-1300, Kureha) binder (85:5:10 in *wt.* ratio) was dispersed in N-methyl pyrrolidone (NMP, Sigma-Aldrich Co.). The resulting slurry was coated on a piece of copper foil (a current collector, thickness = 10 μm). The electrode was pressed with 80% of an initial electrode thickness by a roll-presser, punched out with a diameter of 11 mm and dried at 120^{o}C for 12 h under vacuum.

3.2. Cell preparation

Two-electrode 2032-type coin cells were fabricated with the MCMB composite electrode with lithium foil (as a counter electrode) and glass fiber filter (as a separator, GA-55, Advantec). The standard electrolyte solution was prepared by dissolving 1.0 *M* lithium hexafluorophosphate ($LiPF_6$) in a mixture of ethylene carbonate (EC)/diethyl carbonate (DEC) (1:1 in *vol.* ratio). For a comparative study of the standard electrolyte, the controlling electrolyte solution was prepared by dissolving 1.0 *M* lithium bis(trifluoromethylsulfonyl)imide (LiTFSI) in a mixture of same carbonate solvents.

The cells were assembled in an argon-filled dry box (Model HE-493/Mo-5, Vac. Co.).

3.3. Electrochemical analysis

3.3.1. Charge/discharge cycling

The galvanostatic charge/discharge cycling was made using a WonATech battery cycler (WBCS3000) in a temperature-controlled oven (room temperature, 25^{o}C). Prior to thermal analysis and its electrochemical performances, a pre-cycling step was conducted in order to generate solid electrolyte interphase (SEI) layers on the MCMB electrode satisfactorily. To this end, the galvanostatic charge/discharge cycling was performed for 5 cycles at a current density of 37.2 mA g^{-1} (0.1 C rate, theoretical specific capacity, LiC_6: 372 mA h g^{-1}) in the voltage range of 0.001~2.0 V (*vs.* Li/Li^+). To observe the effect of high-temperature storage on the electrochemical performances, the cells stored at elevated temperature were placed back in a temperature-controlled oven (25^{o}C) and recycled at a same current density in the same voltage range.

3.3.2. Open-circuit voltage (OCV) measurements

To assess the thermal stability of SEI layers on the MCMB electrode, OCV measurements were performed with the cells of various state-of-charges (SOC). For this experiment, the cycling was stopped at the upper cut-off voltage (2.0 V for SOC0

sample) or at the specific capacity cut-off (for SOC25, 50, 75 and 100 samples, SOC100 = 300 mA h g^{-1} in here) after a pre-cycling. And then, the cell was left sufficiently for electrochemical equilibrium. After the cell potential reached the equilibrium value, the Li/MCMB cell was placed in a temperature-controlled oven for high-temperature storage. The OCV was monitored in two different ways; one was to monitor the OCV while the oven temperature was linearly swept from 25^{o}C to 120^{o}C with a ramp rate of 0.1^{o}C min^{-1}. The other while the temperature was fixed at pre-determined temperatures (55^{o}C and 85^{o}C) for various storage times (1, 2, 12, and 24 h).

3.3.3. Galvanostatic intermittent titration technique (GITT)

GITT was employed to obtain the quasi-open-circuit voltage (QOCV) profiles of the MCMB electrodes, in which a current pulse of 37.2 mA g^{-1} was applied for 10 min to measure the closed-circuit voltage (CCV) and turned off for 50 min to obtain the QOCV. The sequential current pulse was applied for both charging and discharging in the range of 0.001~2.0 V (*vs.* Li/Li^{+}).

3.4. Spectroscopic analysis

For post-mortem spectroscopic analyses, the cells were dismantled in an argon-filled dry box. The cycled/stored electrodes were collected and washed with diethyl carbonate (DEC) for eliminating the residue of electrolyte. A home-made hermetic

vessel was used to transfer the electrode samples from dry box to the instrument chamber without air exposure.

3.4.1. Surface analysis

Surface morphology was examined using a field-emission scanning electron microscope (FE-SEM, JSM-6700F, JEOL). The FE-SEM images were collected after platinum sputtering on the MCMB electrodes for enhancing the electron conductivity. To examine the composition of the surface films before/after high-temperature storage, the XPS data were collected in an ultra-high vacuum multipurpose surface analysis system (Sigma probe, Thermo) that operates at a base pressure of < 10^{-10} mbar. The photoelectrons were excited by Al Kα (1486.6 eV) radiation at a constant power of 150 W (15 kV and 10 mA); the X-ray spot size 400 μm^2. During data acquisition, a constant-analyzer-energy mode was used at a pass energy of 30 eV and a step of 0.1 eV. Atomic concentration, which is the ratio of the number of atoms of element of interest to that of others, was calculated by using the following equation [78]:

$$C_x(\%) = 100 \times \frac{n_x}{\sum n_i} = 100 \times \frac{I_x/S_x}{\sum I_i/S_i}$$

Here, the intensity of spectrum of constituent (I_x) is proportional to the number of atoms (n_x) in detection volume and to sensitivity factor (S_x), which characterizes

relative sensitivity of detection of the atom. Since each element has its own sensitivity factor, the number of atoms can be obtained by dividing the intensity of spectrum into sensitivity factor of element of interest. Fitting the XPS data and calculating the atomic concentration are conducted by Thermo Avantage software (*ver.* 4.19).

3.4.2. Structural analysis

The X-ray diffraction (XRD) analysis was made to examine the change of d-spacing (d002 peak) in the MCMB electrodes after high-temperature storage. The XRD patterns were obtained using a D8 diffractometer (Bruker) equipped with Cu Kα radiation (0.154056 nm) and recorded at 40 kV and 40 mA using continuous scanning mode with 3 degree min^{-1}.

4. Results and discussion

4.1. Thermal stability of solid electrolyte interphase (SEI) derived from $LiPF_6$-based electrolyte

Graphite is the most widely used negative electrode material for the lithium-ion batteries (LiBs). One of the characterizations in the graphite negative electrode is considerably low working voltage (< 0.3 V *vs.* Li/Li^+) [2-5]. This provokes 2 drawbacks for LiBs; one is the possibility of lithium dendrite formation, and the other is the inevitability of electrolyte reductive decomposition on the graphite surface. The former can be solved by controlling the current density or voltage cut-off; however, the latter is unavoidable in terms of thermodynamics [74,79,80]. Among the electrolyte solvents, ethylene carbonate (EC) is the most widely used organic solvent in the LiBs. The cathodic stability of EC is not good and decomposition (reduction) voltage is higher than reaction voltage of graphite. Experimentally, the reduction of EC starts from 0.8 V (*vs.* Li/Li^+) during the first lithiation (Fig. 3a). The reductive decomposition of EC fortunately produces the surface film layers on the graphite electrode, so called solid electrolyte interphase (SEI), which passivates the graphite surface to prevent additional carbonate-based organic electrolyte. Fig. 3a shows this characterization of SEI on the MCMB electrode; the voltage plateau (electrolyte decomposition) at 0.7 V (*vs.* Li/Li^+) observed in the first cycle disappeared in the sequent cycles. The differential capacity (dQ/dV) plots obtained in the initial two lithiation processes

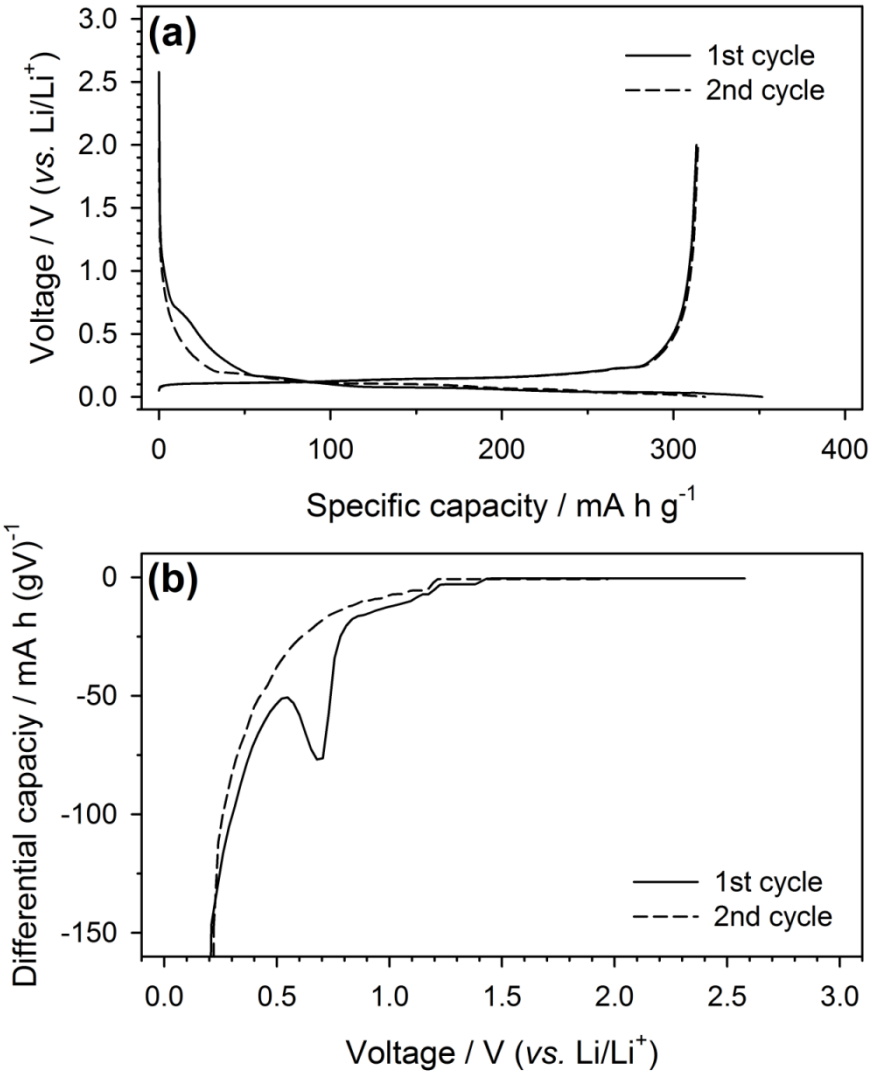

Figure 3. (a) The first and second galvanostatic charge/discharge voltage profiles of the Li/MCMB cell obtained at 25°C. Specific current = 37.2 mA g^{-1}. Voltage cut-off range: 0.001~2 V. (b) Differential capacity (dQ/dV) plots derived from the above-represented voltage profiles.

represent an appearance and disappearance of electrolyte decomposition (Fig. 3b).

The SEI layers are mostly formed in the first cycle. The Coulombic efficiency in the first cycle is approximately 87~89%, and that in the sequent cycle is more than 98%, which means that surface films initially formed plays an excellent role of passivating on the graphite electrode and protecting from additional electrolyte decomposition. After a pre-cycling (5 cycles at a current density of 37.2 mA g^{-1} (0.1 C rate) for the purpose of formation of electrochemically good SEI layers), the surface films covered uniformly on the MCMB electrode (Fig. 4). Compared to pristine electrode (Fig. 4a), surface morphology changed noticeably after a pre-cycling (Fig. 4b). Some cracks or voids were observed scatteredly in the surface films, but SEI layers were well-covered on the graphite electrode and seemed like wet cottons.

The thermal stability of surface film derived from $LiPF_6$-based electrolyte is assessed by monitoring the open-circuit voltage (OCV) during high-temperature storage. Firstly, the OCV variation upon a temperature ramp from 25^{o}C to 120^{o}C is displayed in Fig. 5. The initial value of OCV in the de-lithiated state, SOC0, of the graphite electrode was *ca.* 1.5 V (*vs.* Li/Li^{+}). The OCV remains at the initial value (*ca.* 1.5 V) until 60^{o}C. However, the OCV starts to increase from 60^{o}C to reach a limiting value of 3.0 V, which is the primitive value of pristine graphite electrode. After assembling the cell, the primitive value of OCV is *ca.* 3.0 V and it gradually decreases to reach down to 2.7~2.8 V for wetting period (24 h). Two features should be noted here. First, the initial OCV value (*ca.* 1.5 V), which is lower than the limiting value (*ca.* 3.0 V) for the de-lithiated (SOC0) graphite electrode, reflects that the graphite

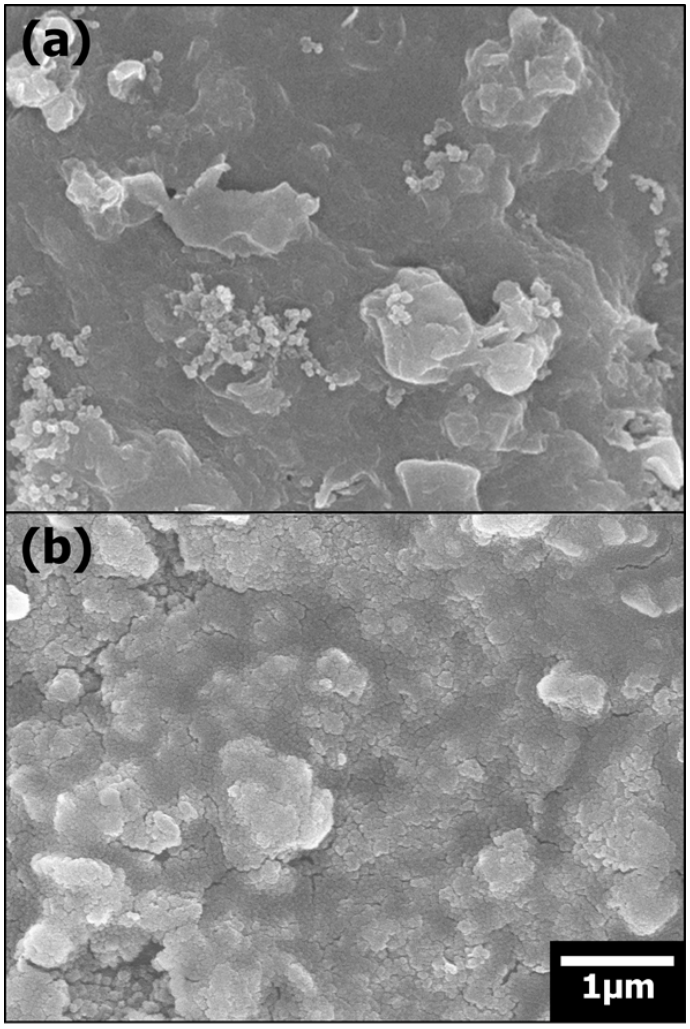

Figure 4. FE-SEM images taken on the surface MCMB electrodes: (a) pristine and (b) after a pre-cycling.

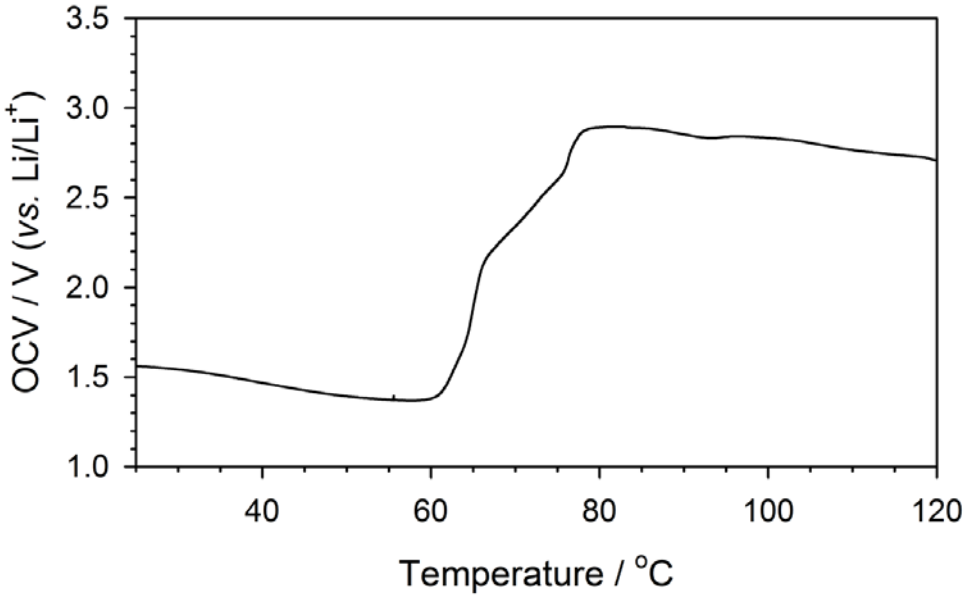

Figure 5. The variation of open-circuit voltage (OCV) of the Li/MCMB cell during high-temperature storage with a temperature ramp of $0.1^{o}C\ min^{-1}$ from $25^{o}C$ to $120^{o}C$.

electrode is not fully de-lithiated ($x < 0.02$ in Li_xC_6), such that the de-lithiation is still possible even if the amount of Li^+ ions/electrons to be removed is very small. Second, the OCV increase is a signature for the oxidation of graphite electrode, during which Li^+ ions and the equivalent amount of electrons are transferred from the graphite electrode to the electrolyte at the interface (de-lithiation reaction). Such a charge transfer is impossible if SEI layers are perfectly passivating on the graphite electrode. Hence, the OCV increase is an indication of a loss of passivating ability, which has resulted from thermal degradation of surface films.

The OCV profile (Fig. 5) can be divided into two regions in the standard point of onset temperature, 60°C; the lower and the higher temperature regions. In the former region, the OCV value remains at 1.5 V (*vs.* Li/Li^+); therefore, SEI layer is relieved from thermal degradation and expected to still have its own passivating ability. In the latter region, however, the OCV increases remarkably and, what is worse, it reaches up to the limiting value of *ca.* 3.0 V. This OCV increase denotes thermal degradation of surface film, which loses its passivating ability. The SEI layer should play a passivating role to suppress additional electrolyte decomposition as an electron insulator. The loss of passivating ability means that the surface film is not functional SEI layer any more but just useless residue of decomposed electrolyte. Therefore, the OCV increase during high-temperature storage can be a barometer to assess the thermal stability of SEI layer, and the former and latter region in the OCV profile (Fig. 5) can be designated as thermally stable and unstable region, respectively. The secondary OCV measurement was conducted during high-temperature fixed at 55°C

and 85°C; those are representatives for each region. As expected, there is little increase of the OCV value during storage at 55°C (thermally stable region), while dramatic OCV increase was observed at 85°C (thermally unstable region) (Fig. 6). Namely, severe thermal degradation occurred to the surface film upon exposure to high-temperature of 85°C, from which it can be inferred that damaged surface film would lose its own passivating ability.

To evaluate the electrochemical properties after storage, the cells are placed back in the RT-controlled oven and recycled. Fig. 7 illustrates the irreversible capacity and Coulombic efficiency before and after high-temperature storage. After storage at 55°C, the Coulombic efficiency and irreversible capacity were 98.7% and 4 mA h g^{-1}, respectively (Fig. 7a). Compared to that before storage, the surface film can still play a passivating role even after storage. On the contrary, the Coulombic efficiency dropped to 84.6% and the irreversible capacity increased to as many as 59 mA h g^{-1} after storage at 85°C (Fig. 7b). Moreover, additional sequent cycles are needed to recover the Coulombic efficiency of more than 99%, which means that continuous irreversible capacity is consumed for several cycles. Namely, the loss of passivating ability from thermal degradation during high-storage at 85°C induces large irreversible capacity and low Coulombic efficiency after storage. The dQ/dV plots obtained before and after storage at 55°C and 85°C are overlapped in Fig. 8. After storage at 55°C, there is no remarkable peak and just similar to that of second cycle, in which SEI layer can prevent additional electrolyte decomposition (Fig. 8a). This indicated that the surface film is still strong to protect the graphite electrode and suppress the electrolyte

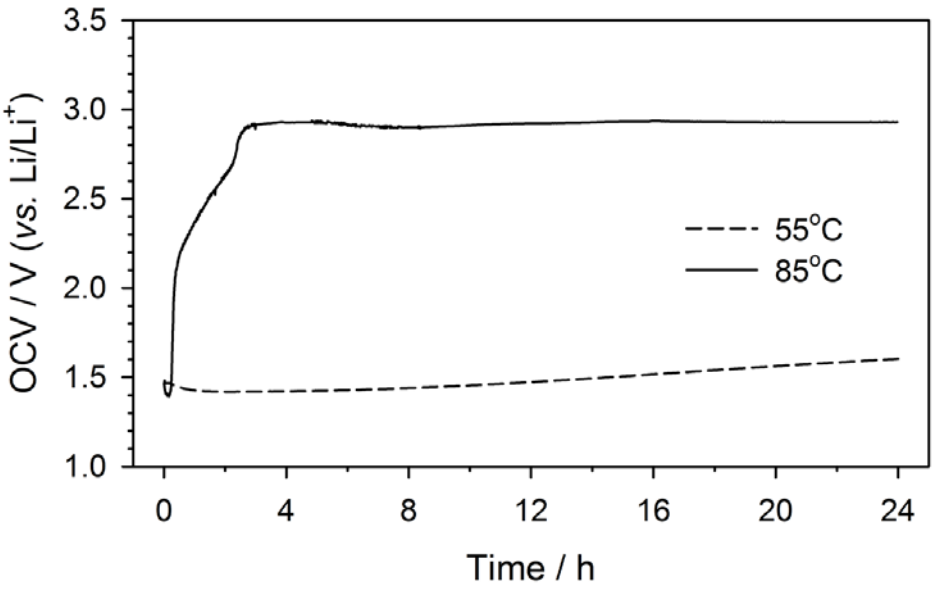

Figure 6. The variation of open-circuit voltage (OCV) of the Li/MCMB cells during high-temperature storage fixed at 55°C (thermally stable) and 85°C (thermally unstable).

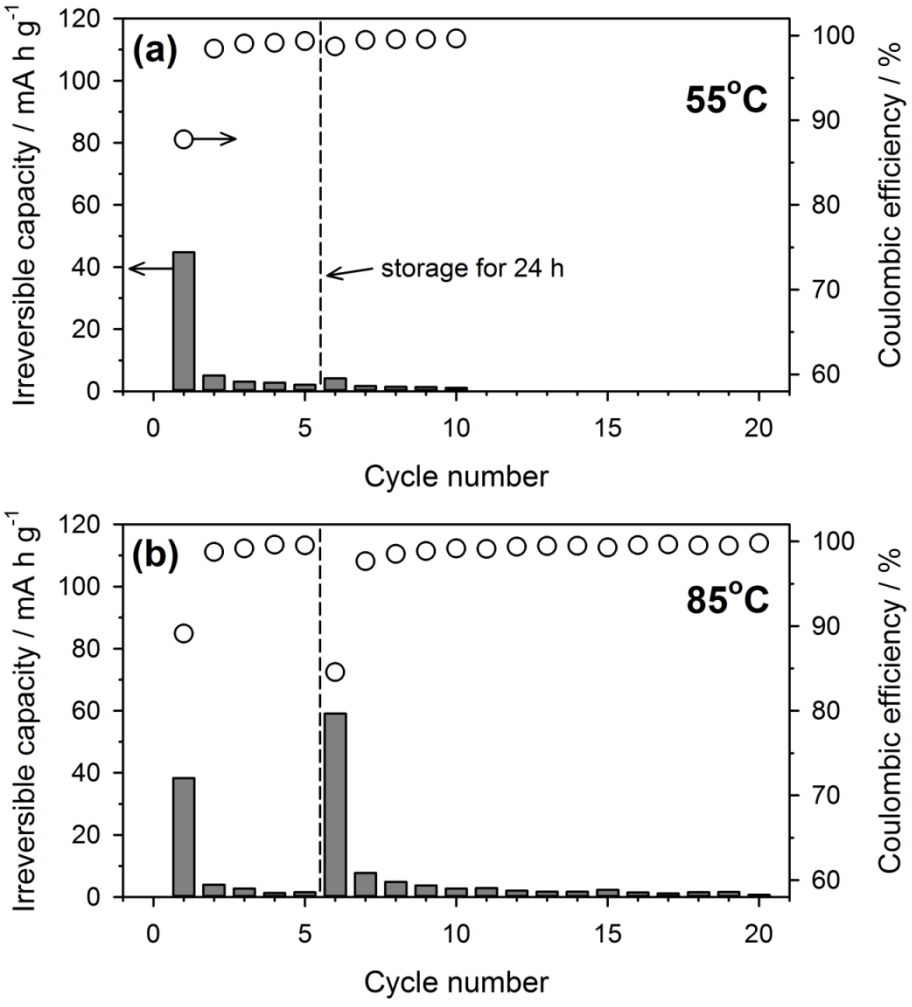

Figure 7. The irreversible capacity and the Coulombic efficiency of Li/MCMB cells before and after high-temperature storage at (a) 55°C and (b) 85°C.

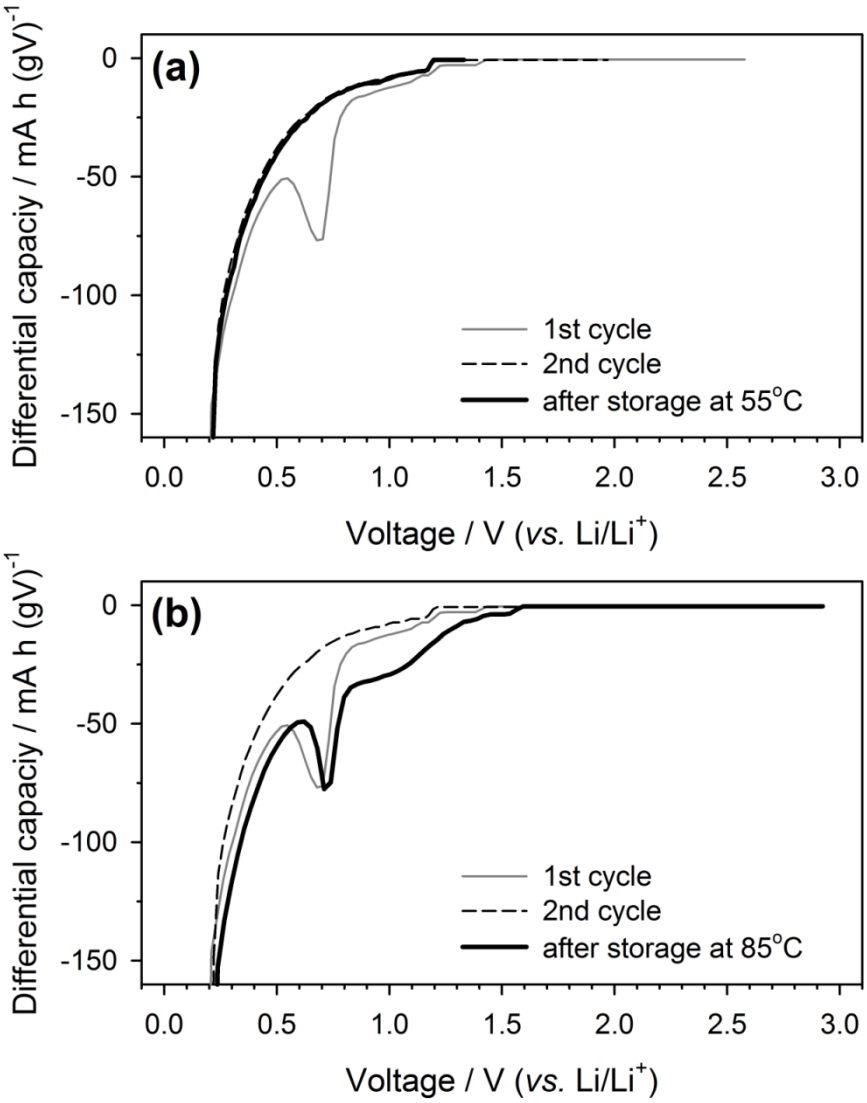

Figure 8. Differential capacity (dQ/dV) plots obtained in the initial two lithiation periods and after high-temperature storage at (a) 55°C and (b) 85°C for 24 h. The galvanostatic charge/discharge was performed at 25°C, from which the dQ/dV profiles were derived.

decomposition to give high Coulombic efficiency (98.7%) even after storage at 55^{o}C (Fig. 7a). The dQ/dV plot shown in Fig. 8b, however, demonstrates that the surface film suffered a severe damage during storage at 85^{o}C. The reductive peak at 0.7 V (*vs.* Li/Li^{+}) from EC decomposition reappears and the intensity of this peak is comparable to that appeared in the first lithiation during a pre-cycling. From the dQ/dV plots (Fig. 8b), the large irreversible capacity observed in Fig. 7b turns out to be originated from the electrolyte decomposition to give low Coulombic efficiency, 84.6%.

Conclusions to be drawn so far are summarized in two phrases; thermal stability and passivating ability. The thermal stability of surface film can be assessed by monitoring the OCV during high-temperature storage. The OCV increase means thermal degradation of surface film. Such thermal degradation leads to the loss of passivating ability and the exposure of MCMB surface. Thermally damaged surface film can no longer protect the surface of graphite electrode and suppress the electrolyte decomposition, which induces the additional electrolyte reduction to give high irreversible capacity and low Coulombic efficiency.

4.2. Thermal behavior of surface films and its effect on electrochemical properties of graphite negative electrode

The SEI derived from $LiPF_6$-based electrolyte is thermally unstable. The surface film suffers from thermal degradation during high-temperature storage at 85^{o}C. The loss of passivating ability causes low Coulombic efficiency in the sequent cycle right

after storage, which is derived from electrolyte decomposition in order to cover passivation film on the MCMB electrode again. Large irreversible capacity consumed to regenerate SEI film is not desirable for cell cycle life, especially in the case of full-cell system. The total amount of lithium (total capacity) is limited to the positive electrode. Namely, limited capacity is forced to be delivered reversibly. The electrolyte decomposition for the SEI formation is inevitable in the first cycle; however, sequent additional electrolyte decomposition should be suppressed in terms of limited total capacity. Therefore, it is essential to elucidate the thermal behavior of surface film during high-temperature storage in order to improve the thermal stability of SEI layers and overcome cell degradation.

Exposure to the temperature of 85^{o}C provokes the thermal degradation of surface film. The value of OCV increases dramatically up to 3.0 V (*vs.* Li/Li^{+}) just in three hours (Fig. 9). Interestingly, the behavior of OCV variation during storage can be divided into two regions: OCV increases in the (i) region and OCV remains at around 3.0 V in the (ii) region. The OCV variation means the change of electron energy in the MCMB electrode, which implies that it is accompanied by the electrochemical reaction. Namely, the electrochemical reaction in addition to the thermal reaction during high-temperature storage are involved in the (i) region. On the other hand, only thermal reaction participates in the (ii) region. It is expected that different thermal behaviors originated from each reaction be observed during high-temperature storage. To elucidate thermal behaviors of each reaction, investigations were conducted separately in each region. Two regions shown in Fig. 9 are hereafter designated by C region and

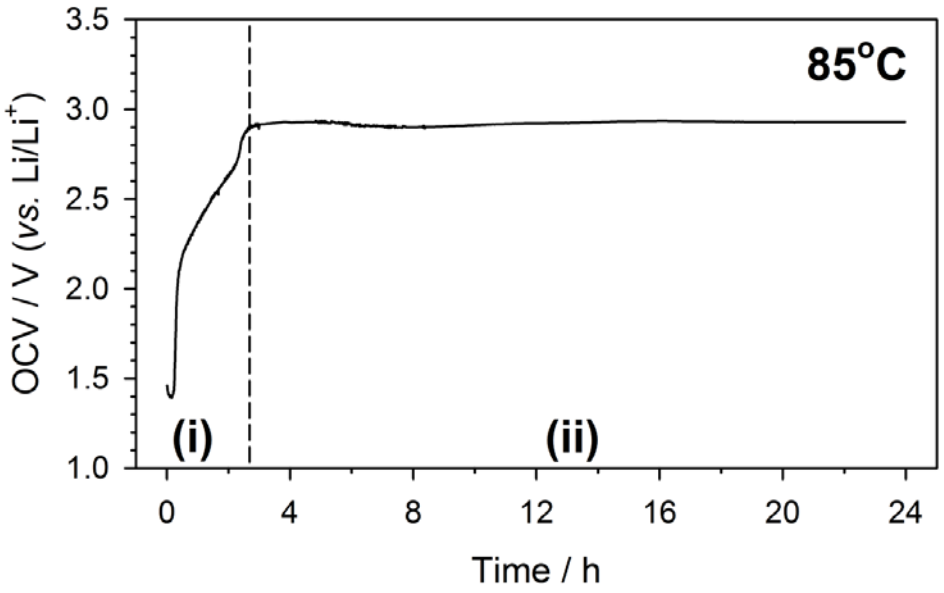

Figure 9. The variation of open-circuit voltage (OCV) of the Li/MCMB cell during high-temperature storage at 85^{o}C for 24 h. (i) C region and (ii) T region.

T region, respectively.

Firstly, the thermal behavior in the C region, where both electrochemical and thermal reactions were involved, was investigated. New variable was controlled with storage time (0, 1, and 2 h). After high-temperature storage at 85^{o}C for each storage time, the cells were placed back in RT-controlled oven and recycled. Fig. 10 shows the irreversible capacity and Coulombic efficiency in the sequent cycle right after storage. The Coulombic efficiency decreases with an increase of storage time; however, the contrary behavior for the irreversible capacity is observed, which implies that longer high-temperature storage results in more severe thermal degradation of surface film. Actually, the increased irreversible capacity upon storage time is originated from the electrolyte decomposition (Fig. 11). The dQ/dV profiles in Fig. 11b compare the intensity of each reductive peak at 0.7 V (*vs.* Li/Li^{+}). The peak starts to protrude after storage for 1 h and increases upon storage time, which indicates that long exposure to elevated temperature provokes more severe thermal degradation of surface film and the exposure of MCMB surface.

The loss of passivating ability due to thermal degradation is further confirmed by observing the SEM images taken after high-temperature storage. Fig. 12a shows the SEM image of pristine electrode surface. After a pre-cycling (before storage), the foreign materials are deposited on the graphite electrode surface, which must be SEI derived from electrolyte decomposition (Fig. 12b). After high-temperature storage, however, the deposited surface films are degraded to be crumbling and getting rough upon storage time (Figs. 12c and 12d). The damaged surface film loses its original

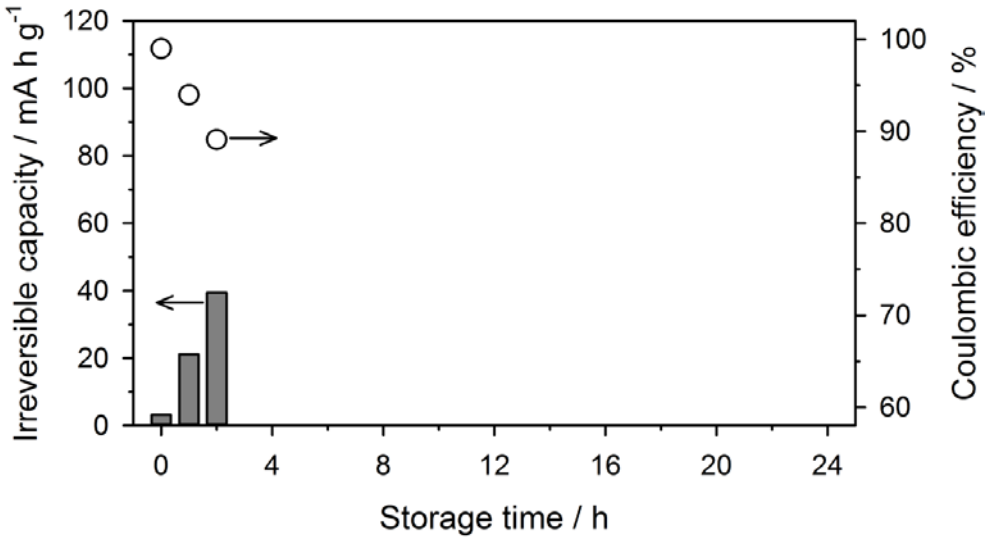

Figure 10. The irreversible capacity and the Coulombic efficiency of Li/MCMB cells after high-temperature at 85^{o}C storage for 0 (before storage), 1, and 2 h.

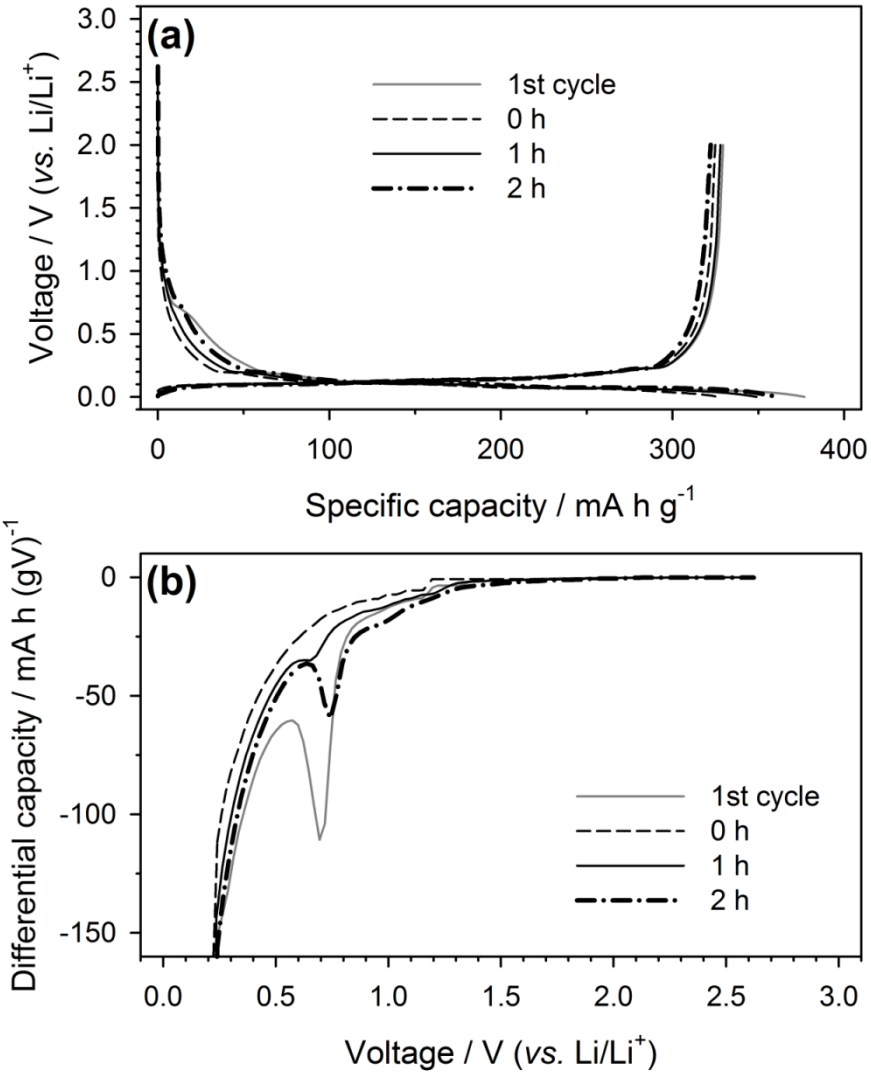

Figure 11. (a) The galvanostatic charge/discharge voltage profiles of the Li/MCMB cells obtained at 25°C in the first cycle and after high-temperature storage at 85°C. Specific current = 37.2 mA g^{-1}. Voltage cut-off range: 0.001~2 V. (b) Differential capacity (dQ/dV) plots derived from the above voltage profiles.

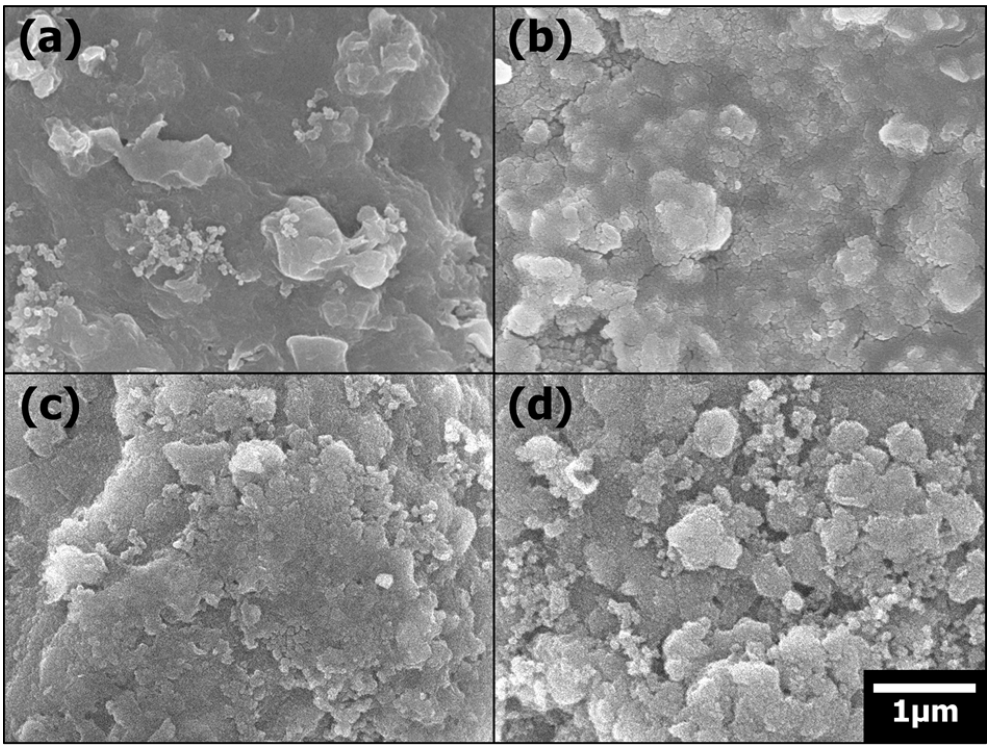

Figure 12. FE-SEM images taken on the surface MCMB electrodes: (a) pristine, (b) before storage (after a pre-cycling), and after high-temperature storage at 85^{o}C for (c) 1 h, and (d) 2 h.

surface morphology, from which it can be deduced that surface morphology is associated with the passivating ability of surface films. On the other hand, it is hardly to observe the MCMB electrode surface directly in the SEM images taken after high-temperature storage. Thanks to X-ray photoelectron spectroscopy (XPS) analysis, the evidence of the MCMB surface exposure is found. All the XPS spectra were fitted according to the reported binding energy in Table 1. Fig. 13 displays the C 1s spectra taken from the MCMB electrode before and after high-temperature storage. In the pristine electrode, two distinguished peaks from hydrocarbon (C-C and C-H) and PVdF (CF_2) are observed. The intensity of two peaks, however, decreases after SEI formation. Moreover, the peak at 285 eV loses its shape of sharpness. These features seem to be originated the deposited films on the surface of the graphite negative electrode. It can be ascertained whether the surface films are covered or not by observing the shape of these two peaks of C 1s spectra. After high-temperature storage for 2 h, the hydrocarbon peak is recovered to be sharp like that of pristine electrode, which is a convincing evidence of MCMB surface exposure from thermal degradation.

To gain an insight into the thermal behavior of SEI films, the film compositions are analyzed by using XPS. The XPS data taken before and after high-temperature storage are analyzed (Fig. 14). The chemical transformation is confirmed on the O 1s spectra (Fig. 14a). As seen, surface film after the high-temperature storage gives rise to a higher intensity for the carbon-oxygen species at 533.5 eV. The intensity of main peak at 532 eV before storage diminishes, which indicates that the original SEI film is thermally degraded during high-temperature storage. In chemistry, a double bond

Table 1. Peak assignment of each element obtained from XPS spectra of the graphite electrode before and after high-temperature storage at 85°C [29,81-84].

Element	Assignment	Binding energy (eV)
C 1s	Graphite or carbon black	284.2
	Hydrocarbon (C-C and C-H)	285.0
	C-O	286.5
	O-C-O or C=O	287.6
	O=C-O	289.0
	$ROCO_2Li$ or Li_2CO_3	290.3
	CF_2 (PVdF)	291.2
	CF_3 (LiTFSI)	293.0
O 1s	Li_2O	528
	O-C=O or Li_2CO_3	532
	O-C=O	533.5
	$Li_xPF_yO_z$	535
F 1s	LiF	685
	$Li_xPF_yO_z$	686.6
	$LiPF_6$ or CF_2 (PVdF)	688.5
	CF_3 (LiTFSI)	688.6

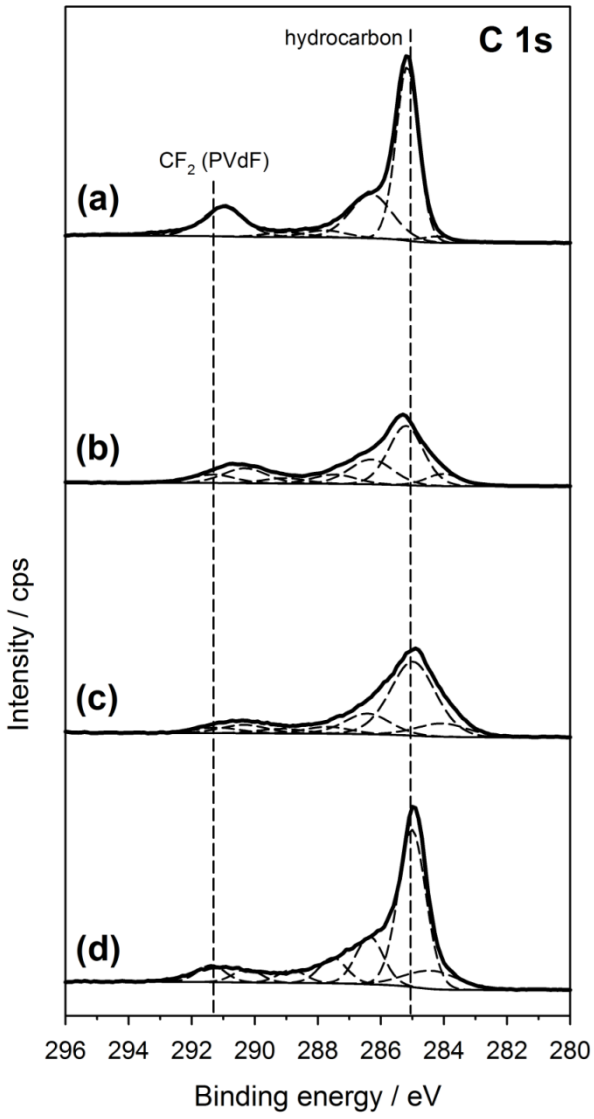

Figure 13. C 1s XPS spectra obtained from the MCMB electrodes: (a) pristine, (b) before storage (after a pre-cycling), and after high-temperature storage at 85^{o}C for (c) 1 h, and (d) 2 h.

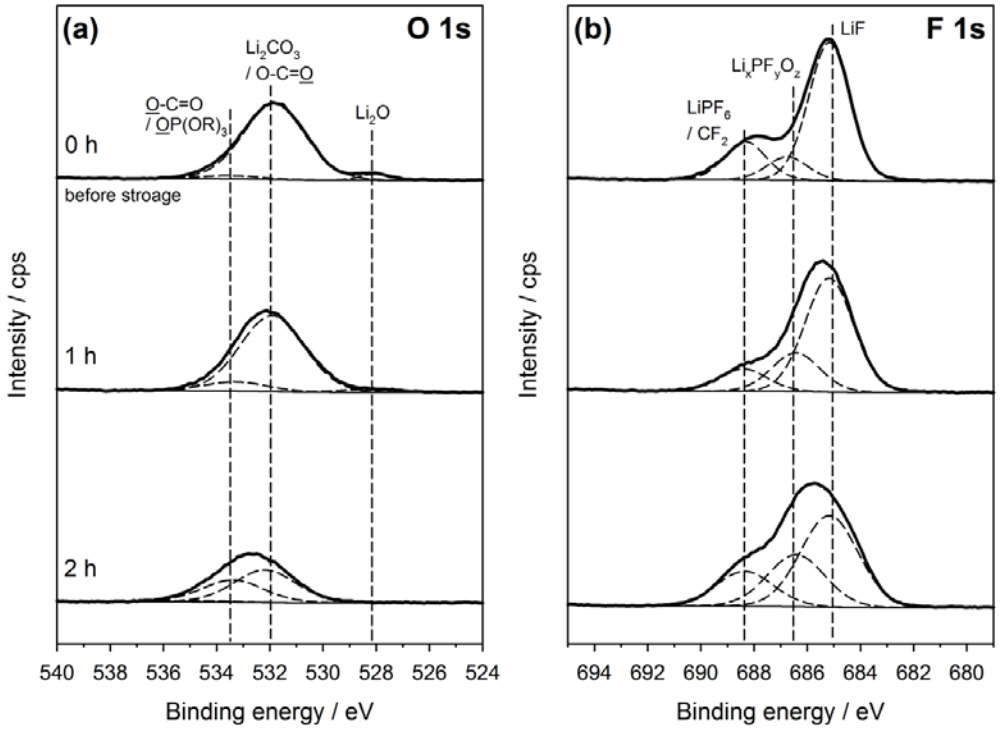

Figure 14. (a) O 1s and (b) F 1s XPS spectra obtained from the MCMB electrodes before storage (after a pre-cycling) and after high-temperature storage at 85°C for 1 and 2 h.

(electron-rich) is more reactive than a single bond (electron-deficient). Therefore, long exposure to elevated temperature enables to transform the chemical species with double-bonds easily. And also, high population of F-containing species in the surface films after storage is observed in F 1s spectra (Fig. 14b). The population of LiF is dominant over the other F-species before storage; however, the evolution of $Li_xPF_yO_z$, products of salt decomposition, increase upon high-temperature storage. $LiPF_6$ salt in non-aqueous solution is known to be decomposed at 70^oC and produces LiF(s) and PF_5(g), of which gaseous PF_5 easily reacts with carbonate solvents [74,85]. Decomposed products of $LiPF_6$ salts are deposited on the damaged surface films and contributed to high population of F-containing species.

So far, the thermal behavior of the surface film in the C region is investigated. It was expected that both electrochemical and thermal reaction would be involved in this region. Unlike expected, however, only thermal degradation from the thermal reaction is observed. Two possibilities should be considered. One is that the thermal reaction is actually overwhelming the electrochemical reaction during high-temperature storage. The electrochemical reaction accompanied by charge transfer could be buried under significant thermal reaction to deteriorate the surface film and lithium salt. The other possibility is that consumed electrons are so small that the electrochemical reaction hardly participates in the thermal behavior of surface film. Practically, for the de-lithiated (SOC0) state, the graphite electrode contains a little amount of lithium ions/electrons ($x < 0.02$ in Li_xC_6). Compared to the capacity for SEI formation, its amount seems to be not large enough to involve in the thermal behavior. To investigate

the contribution of the electrochemical reaction to thermal behavior, the graphite negative electrodes are prepared with various SOC (state-of-charge) states; SOC0, SOC25, SOC50, SOC75, and SOC100 (in here, SOC100 = 300 mA h g^{-1}) (Fig. 15).

The thermal behavior of each sample was observed using the OCV measurement during high-temperature storage at 85^{o}C. The OCV value of all the samples increases upon storage time (Fig. 16). The deviation between initial and final values during high-temperature storage is, of course, different. According to the extent of OCV increase, the samples can be divided into two groups: One (SOC0 and SOC25) is OCV up to 3.0 V (*vs.* Li/Li^{+}) and the other (SOC50, SOC75, and SOC100) is OCV under 3.0 V, a limiting value. The former group has no electron to be released from electrode, so the thermal behavior affected by only thermal reaction can be observed. The latter group, however, is still under the limiting value of 3.0 V, which means they have extra lithium ions/electrons after storage. The former and latter group, hereafter, can be designated as T group and C group, respectively. To understand the relationship between OCV and consumed capacity, two analyses are conducted. XRD patterns are recorded before and after high-temperature storage (Fig. 17). Generally, lithium ion is intercalated/de-intercalated into/from graphine layers. The distance of these layers (d002 = 0.336 nm) expands/contracts with lithium intercalation/de-intercalation. The main peak at 26.5^{o} of pristine graphite electrode represents the distance of graphine layers. The shift to low/high angle means lithium intercalation/de-intercalation into/from graphine layers. For all the samples, the d002 peak is shifted from low angle to high angle after high-temperature storage, which means lithium de-intercalation from graphine layers. The

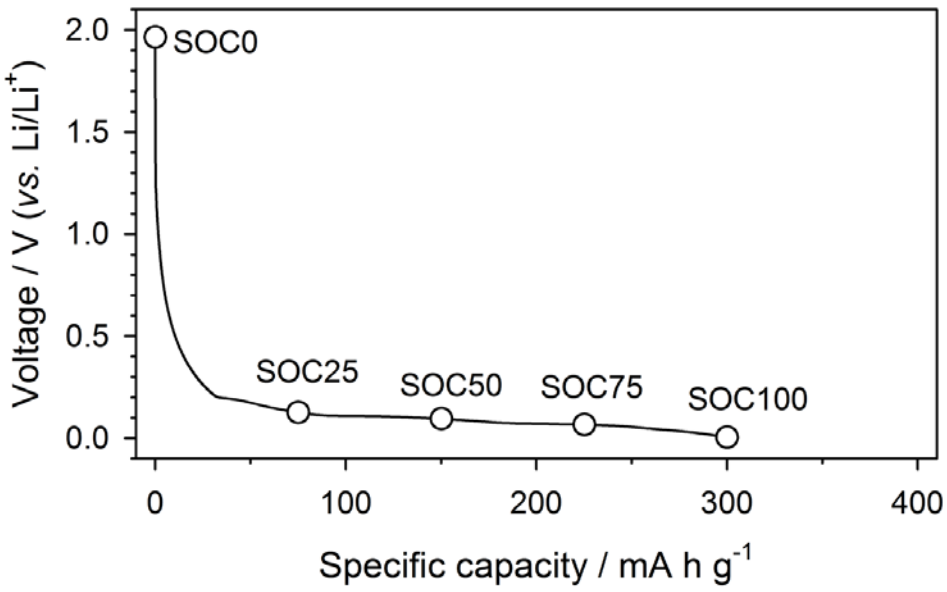

Figure 15. The galvanostatic charge (lithiation) voltage profile of the Li/MCMB cell obtained at 25°C. Specific current = 37.2 mA g^{-1}. Marks on the SOC0, SOC25, SOC50, SOC75, and SOC100 (in here, SOC100 = 300 mA h g^{-1}).

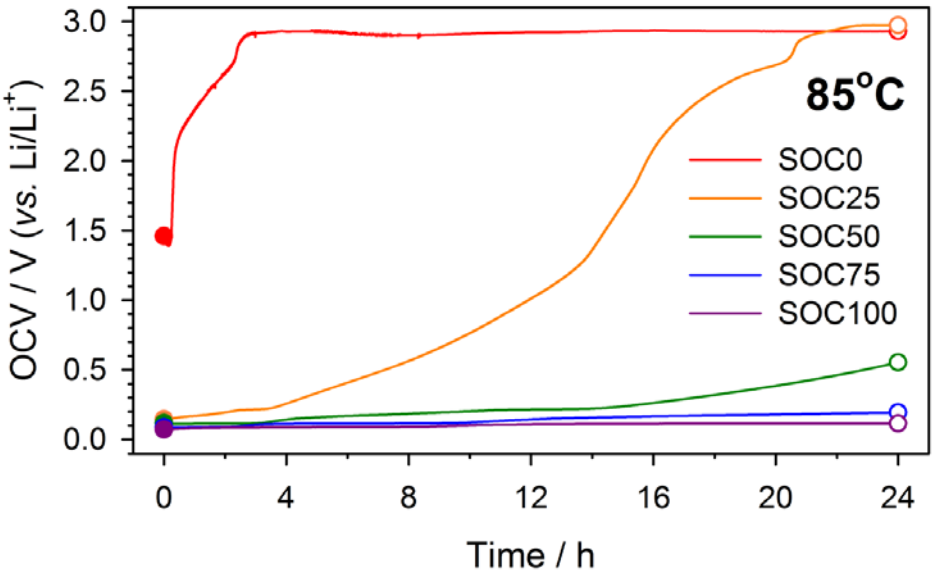

Figure 16. The variation of open-circuit voltage (OCV) of the Li/MCMB cell during high-temperature storage at 85°C.

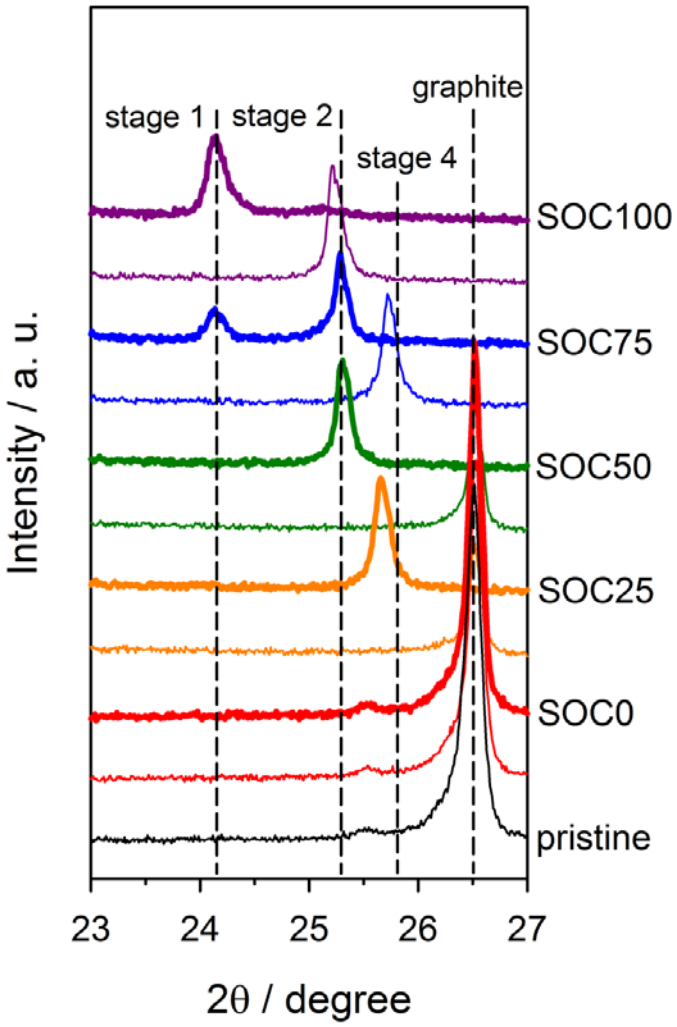

Figure 17. XRD patterns obtained from the MCMB electrodes before (bold solid lines) and after (thin solid line) high-temperature storage at 85°C for 24 h.

XRD patterns roughly introduce loss of lithium ions/electrons during high-temperature storage; however, it cannot offer exact amount of consumed capacity.

To measure consumed capacity using the values obtained from the OCV measurement (Fig. 16), galvanostatic intermittent titration technique (GITT) was conduct after a pre-cycling (Fig. 18a). From the GITT profile, the close-circuit voltage (CCV) and quasi-open-circuit voltage (QOCV) profiles are plotted separately (Fig. 18b). Applying the initial and final OCV values obtained from the OCV measurement (Fig. 16) to QOCV profile can help to understand the relationship between the OCV and consumed capacity (Fig. 19). Two features should be noted here. First, large increase of OCV value cannot always lead to loss of large electrons. If the initial value of OCV is same, such a conclusion would be reasonable. Second, the C group consumes more capacity than the T group during high-temperature storage. This tendency is fairly consistent with that of direct capacity measuring; the subtraction of de-lithiation capacity after storage from lithiation capacity before storage. Fig. 20 displays the galvanostatic charge/discharge profiles before and after high-temperature storage. Consumed capacity (or lithium ions/electrons) for all the samples can be calculated: < 8, 75, 139, 167, and 168 mA h g^{-1}, respectively. Based on the OCV variation and consumed capacity, the samples are reduced to only three of SOC0, SOC25, and SOC50.

Fig. 21 shows the OCV variation of three samples with SOC0, SOC25, and SOC50 during high-temperature storage at 85^{o}C. Samples of 12 h and 24 h-storage are further established for specific investigation and marked on the OCV profiles: SOC0s and

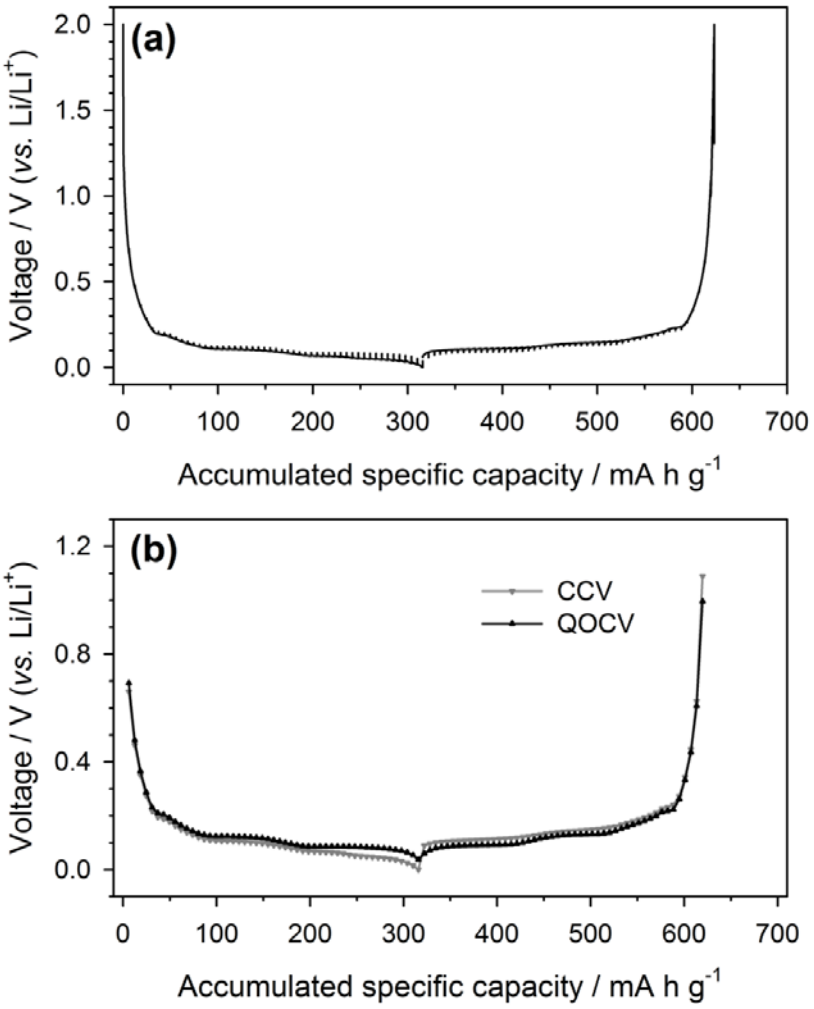

Figure 18. (a) The galvanostatic intermittent titration technique (GITT) voltage profile obtained with the Li/MCMB cell after a pre-cycling. (b) closed-circuit voltage (CCV) and quasi-open-circuit voltage (QOCV) profiles derived from the above-represented GITT voltage profile.

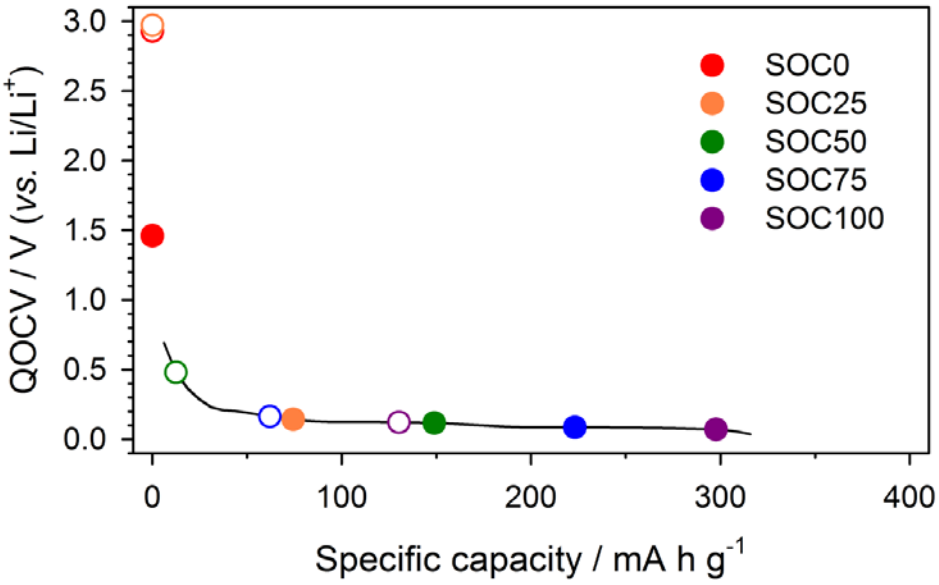

Figure 19. The OCV variation on the quasi-open-circuit voltage (QOCV) profile before (circle) and after (empty circle) high-temperature storage at 85°C for 24 h.

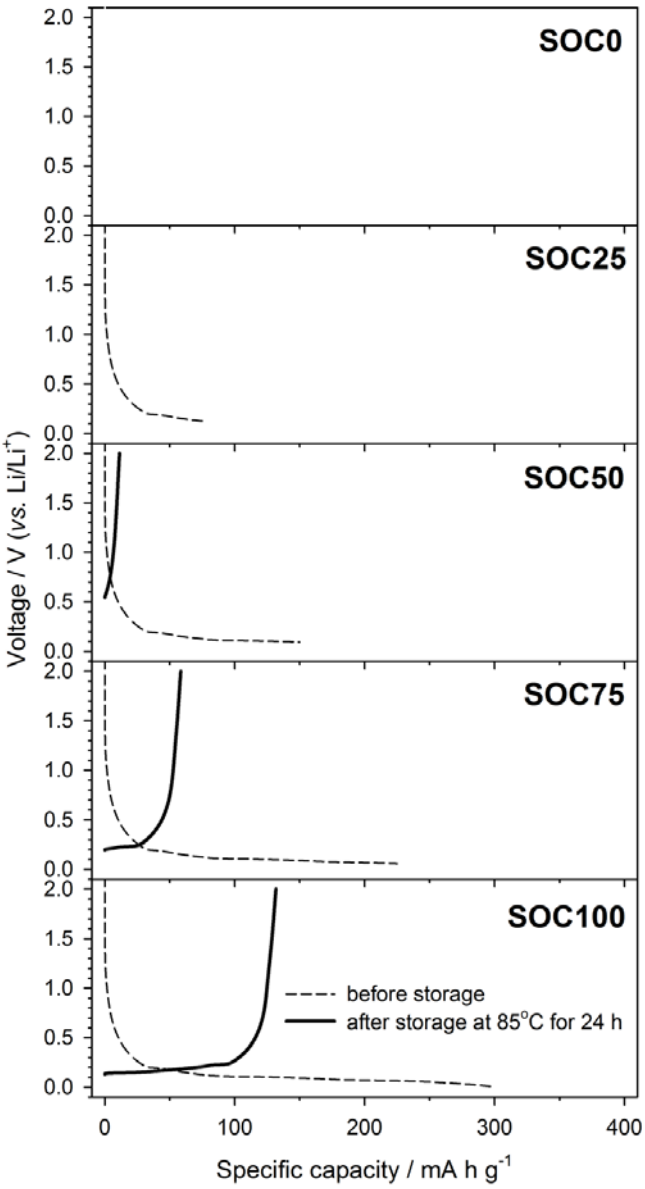

Figure 20. The galvanostatic charge/discharge voltage profiles of Li/MCMB cells before (dash line) and after (solid line) high-temperature storage at 85°C for 24 h.

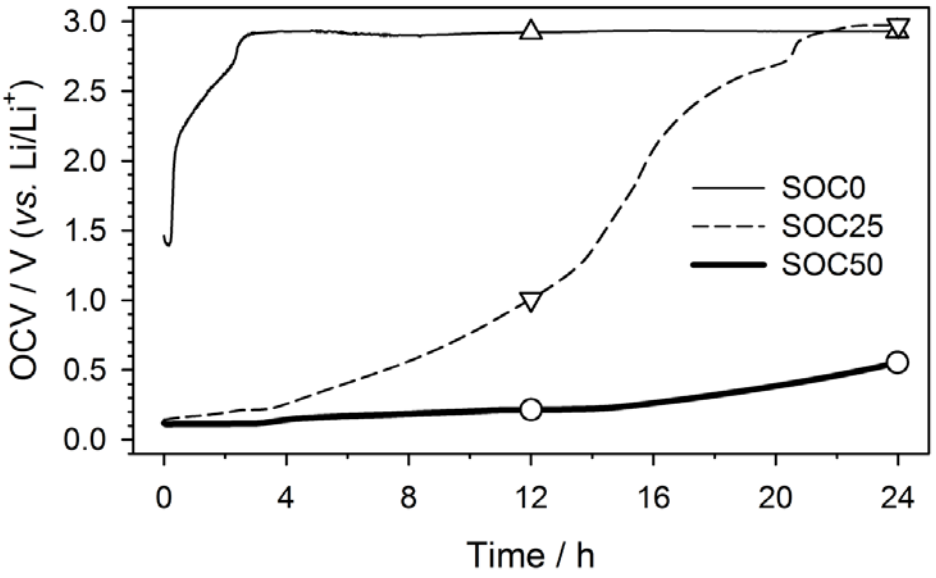

Figure 21. The variation of open-circuit voltage (OCV) of Li/MCMB cells during high-temperature storage at 85°C for 24 h. Marks on 12 h and 24 h-storage time for SOC0, SOC25, and SOC100.

SOC25 of 12 h-storage in T group and SOC25 of 24 h-storage and SOC50s in C group.

After high-temperature storage at 85^{o}C, the cells were placed in RT-controlled oven and recycled and its irreversible capacity and Coulombic efficiency are displayed in Fig. 22. The low Coulombic efficiency and high irreversible capacity are observed in the T group; however, the contrary results are released in the C group. In the galvanostatic charge/discharge voltage profiles and their dQ/dV plots displayed in Figs. 23 and 24, different electrochemical behaviors are observed in each group. In the T group (both SOC0s and SOC25 of 24 h-storage), the voltage plateau and reduction peak at around 0.7 V (*vs.* Li/Li^{+}) was observed (Figs. 23 and 24b). This voltage plateau (reduction peak) is originated from the reductive decomposition of electrolyte, which induces that the surface films in T group lost its passivating ability due to thermal degradation. Meanwhile, no voltage plateau (reduction peak) derived from electrolyte decomposition is observed in C group (Figs. 23 and 24a). Their surface films seem to still play a good passivating role after high-temperature storage.

One obvious conclusion to be drawn here is that the surface films of C group are influenced dominantly by the electrochemical reaction during high-temperature storage. Namely, the damaged surface films from thermal degradation turn out to be restored. The OCV increase and consumed capacity during storage are apparent evidences for thermal degradation, which implies that the surface films preferentially suffered from the thermal reaction. Nonetheless, their surface films still play a good passivating role to suppress electrolyte decomposition in the sequent cycle right after high-temperature storage (Figs. 23 and 24a).

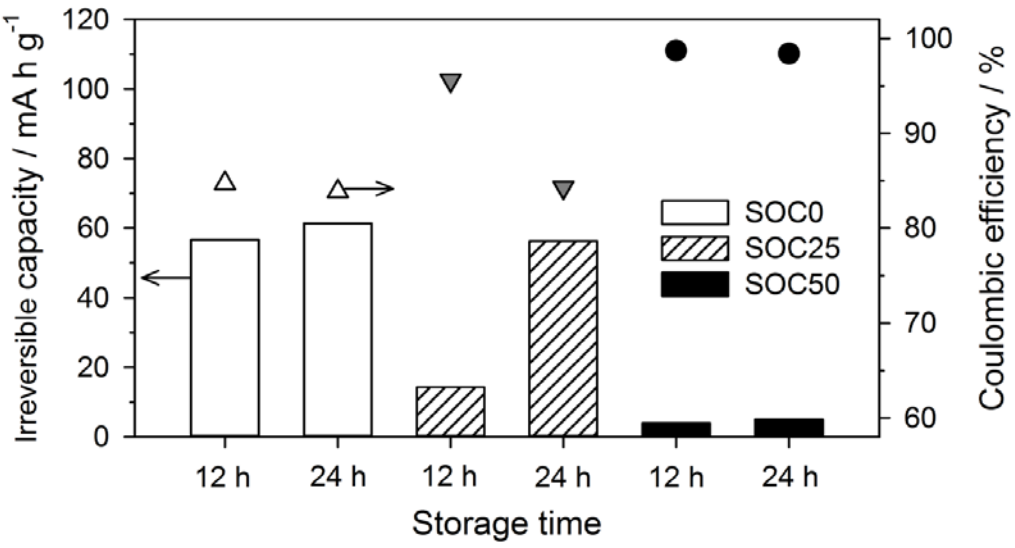

Figure 22. The irreversible capacity and the Coulombic efficiency of Li/MCMB cells after high-temperature at 85°C storage for 12 h and 24 h.

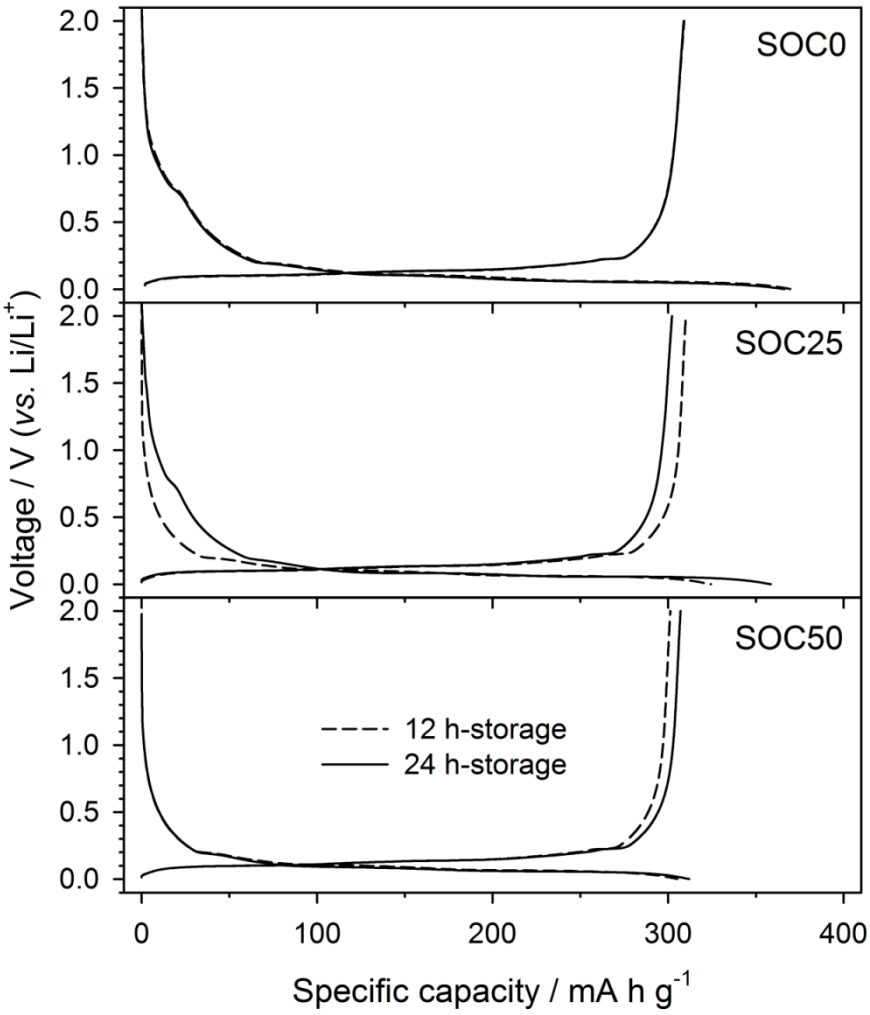

Figure 23. The galvanostatic charge/discharge voltage profiles of Li/MCMB cells obtained at 25°C after high-temperature storage at 85°C for 12 h (dash line) and 24 h (solid line). Specific current = 37.2 mA g^{-1}. Voltage cut-off range: 0.001~2 V.

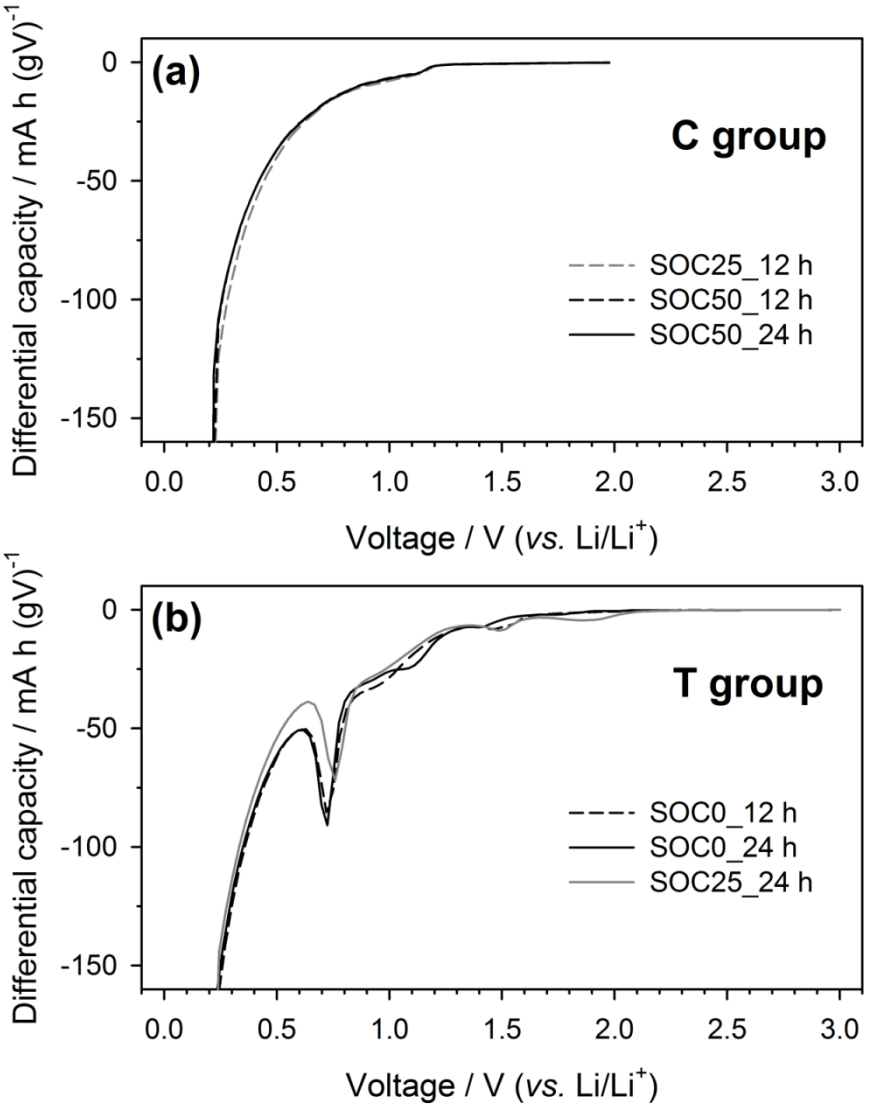

Figure 24. Differential capacity (dQ/dV) plots obtained after storage at 85°C for 12 h and 24 h. The galvanostatic charge/discharge was performed at 25°C, from which the dQ/dV profiles were derived. (a) C group and (b) T group.

To elucidate thermal behavior of the surface films in the C group, the FE-SEM and XPS analyses are conducted. The SEM images taken after high-temperature storage are shown in Fig. 25. For the SOC0s (the T group), the surface films are already damaged to be crumbled extremely and lose the original shape compared to that before storage (Figs. 25c and 25d). The surface obtained in the SOC50s (the C group) looks totally different from that in the SOC0s. The surface films seem to still remain their original wet-cotton-like shape and uniformity (Figs. 25g and 25h). Compared to the initial SEI films, however, their morphology looks different as if some foreign materials are deposited on the surface. Namely, surface films in the C group are regenerated by the electrochemical reaction. After the thermal degradation of surface films, loss of electrons and lithium ions contributes to reform the damaged surface film. The high SOC samples contain sufficiently large amount of electrons before storage. Due to the thermal degradation, electrons in the graphite electrode could transfer to and react with electrolyte, which induces the reformation of surface films. The SEM images of the SOC25s give positive proof of this conclusion (Figs. 25e and 25f). After 12 h-storage, the surface starts to be crumbled but still remains its own coverage characteristic since consumed capacity is enough to reform the damaged surface films. After another 12 h-storage, however, it turns out that the surface films are damaged severely and chunks observed from Fig. 25e are broken into little particles, which can be inferred that the thermal reaction (that is, thermal degradation) is dominant (Fig. 25f).

The chemical compositions of regenerated surface films by the electrochemical reaction during high-temperature storage were identified using XPS. The features of

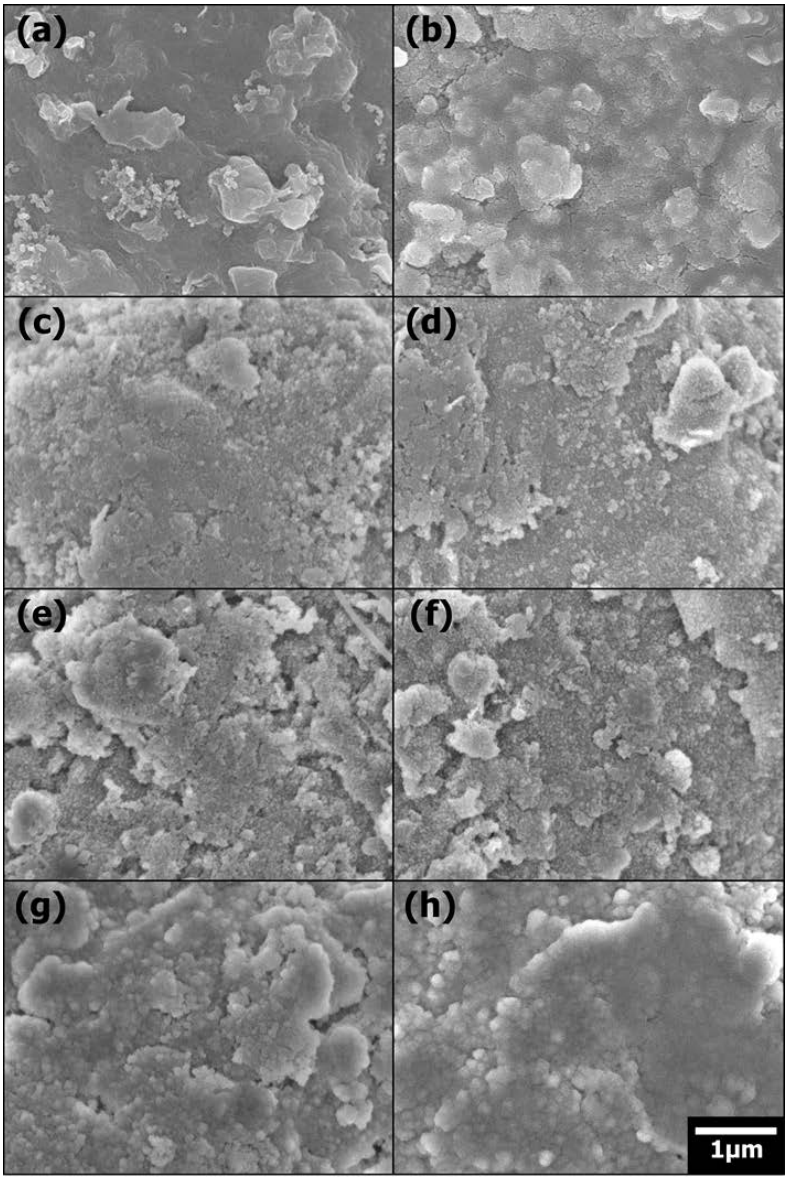

Figure 25. FE-SEM images taken on the surface MCMB electrodes: (a) pristine, (b) before storage (after a pre-cycling), (c)/(e)/(g) after storage at 85^{o}C for 12 h, and (d)/(f)/(h) after storage at 85^{o}C for 24 h. Note that SOC0/SOC25/SOC50 in order.

damaged surface films from thermal degradation are mentioned above; the chemical transformation from carbon-oxygen species with double bonds in the O 1s spectra and the high population of decomposed products from lithium salts in the F 1s spectra (Fig. 14). Such characteristics are observed in the XPS spectra of the T group (Figs. 26a, 27a, 28a, 28b, 29a and 29b). The surface films in the C group, however, show chemically compositional similarity with the original SEI films derived from EC decomposition in the first cycle (Figs. 26b, 26c, 27b, 27c, 28c and 29c), from which it can be deduced that the consumed electrons/lithium ions (capacity) reacted with EC solvent to repair the damaged surface films from thermal degradation during high-temperature storage. EC reductive decomposition is thermodynamically possible since the OCV value in the C group is beyond the cathodic electrochemical stability windows of electrolyte. On the other hand, additional peaks at high binding energy appear in both O 1s and F 1s spectra for the SOC0 of 24 h-storage (Figs. 28a and 29a). Compared to those for the SOC0 of 12 h-storage (Figs. 26a and 27a), the population of decomposed products from lithium salts increases remarkably, which can be inferred that longer storage time at elevated temperature induces continuous lithium salt decomposition by the thermal reaction.

In conclusion, all the features in thermal behaviors of surface films are summarized in a schematic diagram (Fig. 30). After a pre-cycling, SEI films are formed on the graphite negative electrode. The SEI films play a passivating role to prevent additional electrolyte decomposition. The elevated-temperature storage, however, provokes thermal degradation of surface films. The thermally damaged surface film loses its own

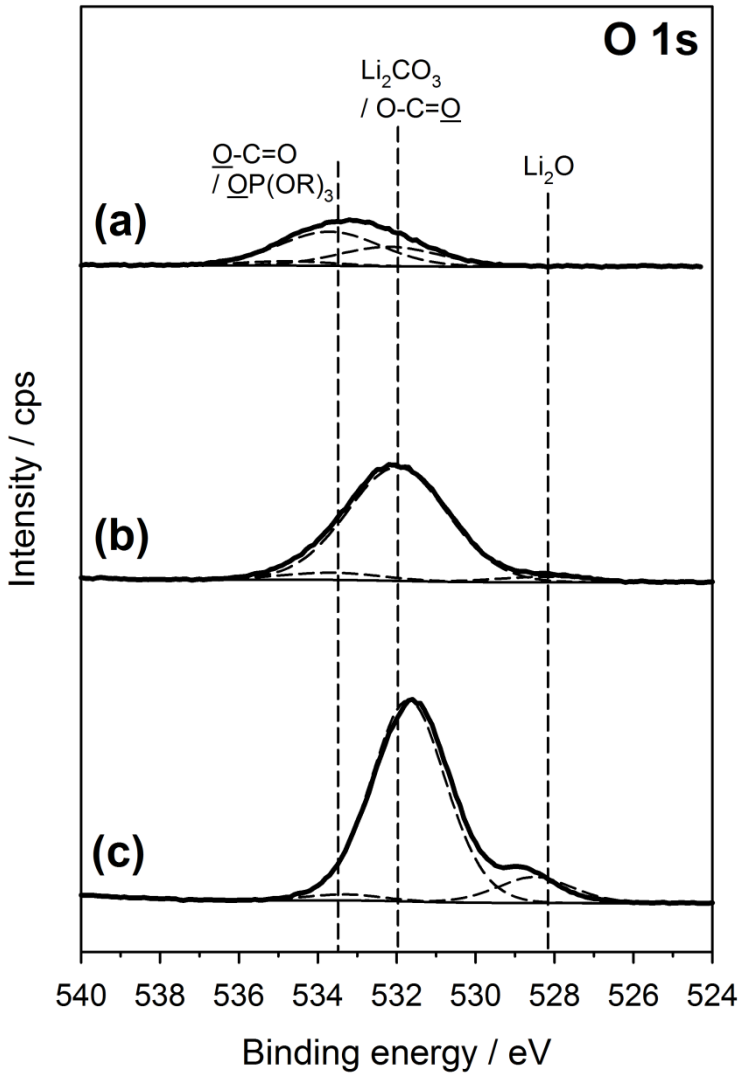

Figure 26. O 1s XPS spectra obtained from the MCMB electrodes after high-temperature storage at 85°C for 12 h. (a) SOC0, (b) SOC25, and (c) SOC50.

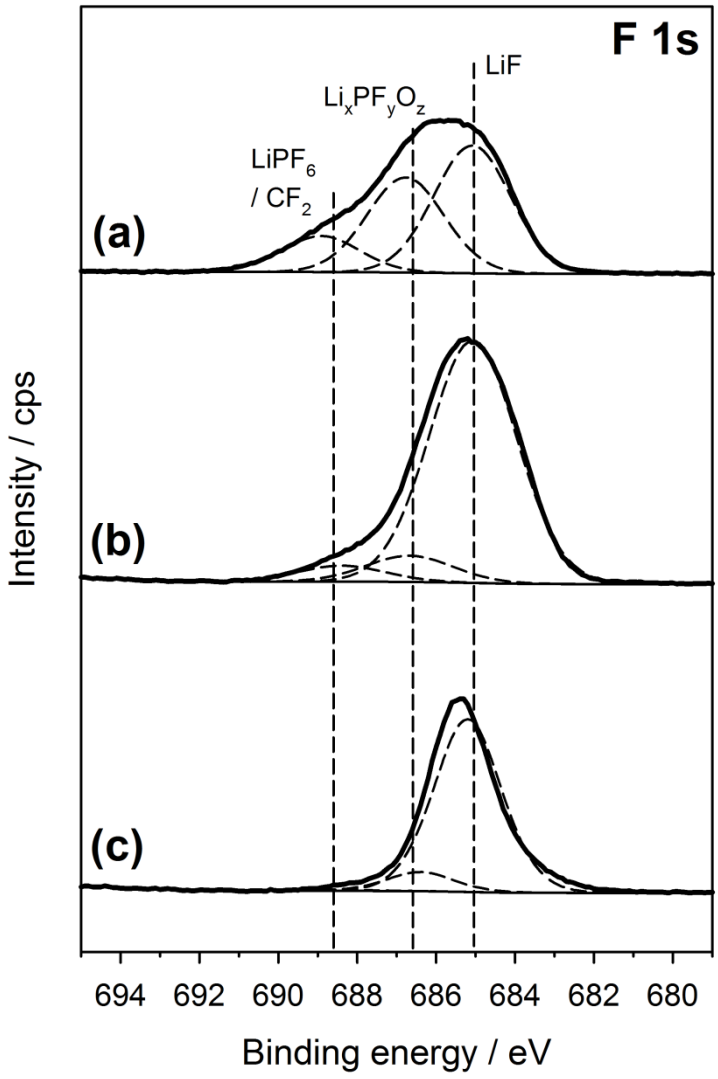

Figure 27. F 1s XPS spectra obtained from the MCMB electrodes after high-temperature storage at 85°C for 12 h. (a) SOC0, (b) SOC25, and (c) SOC50.

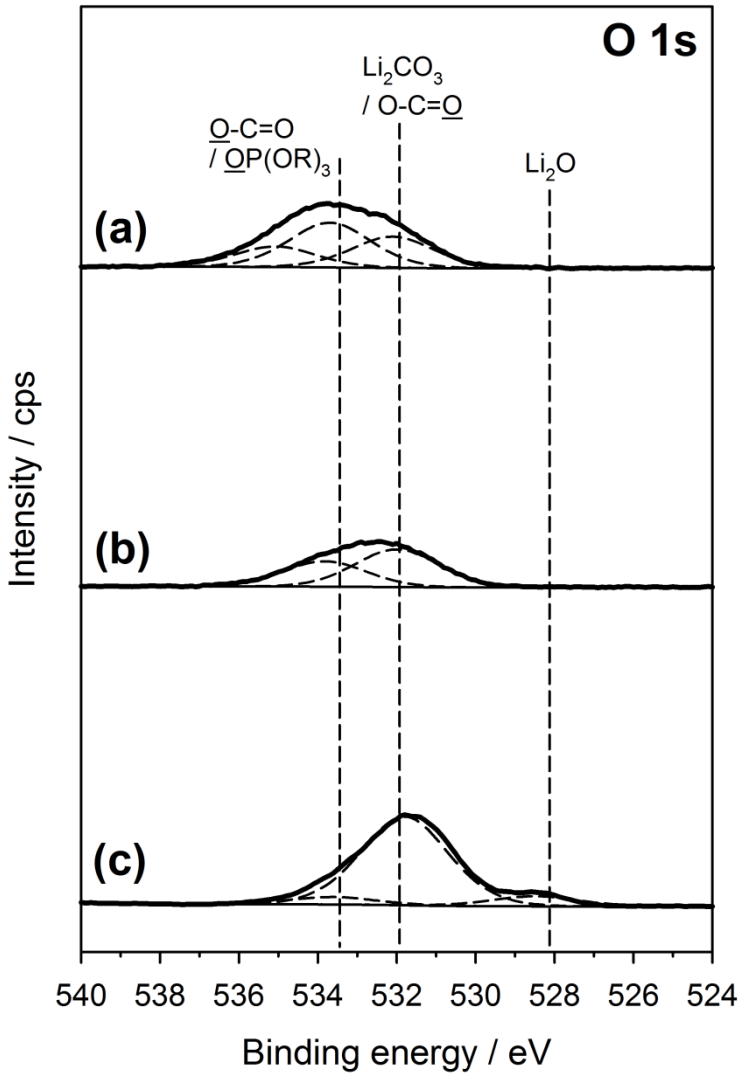

Figure 28. O 1s XPS spectra obtained from the MCMB electrodes after high-temperature storage at 85°C for 24 h. (a) SOC0, (b) SOC25, and (c) SOC50.

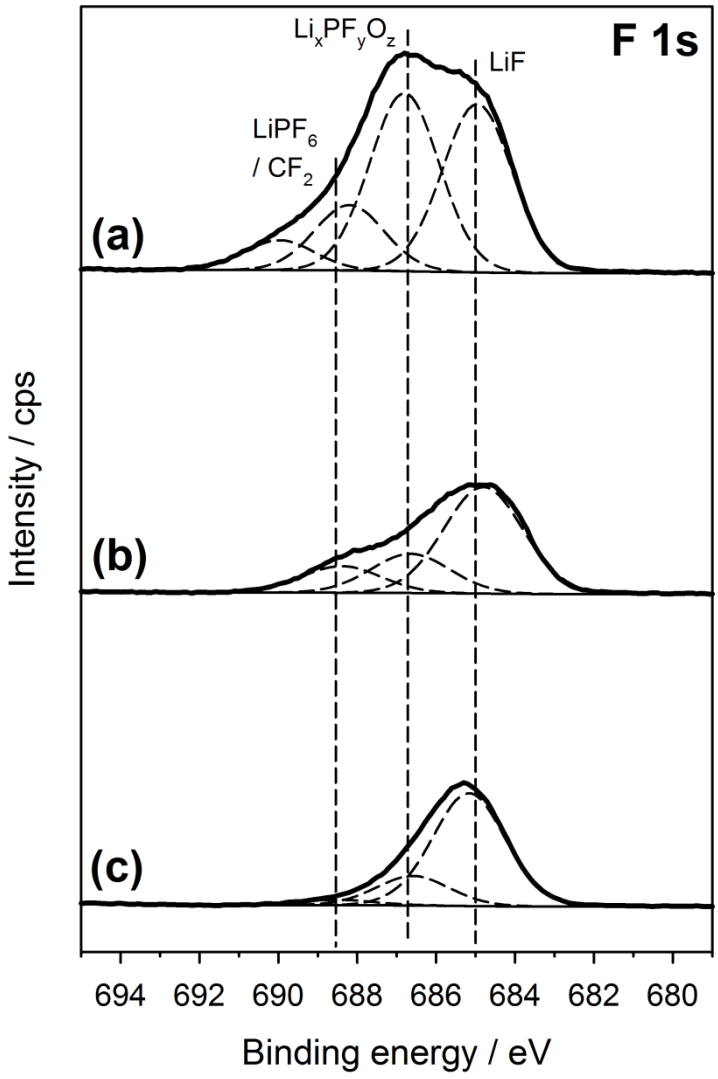

Figure 29. F 1s XPS spectra obtained from the MCMB electrodes after high-temperature storage at 85°C for 24 h. (a) SOC0, (b) SOC25, and (c) SOC50.

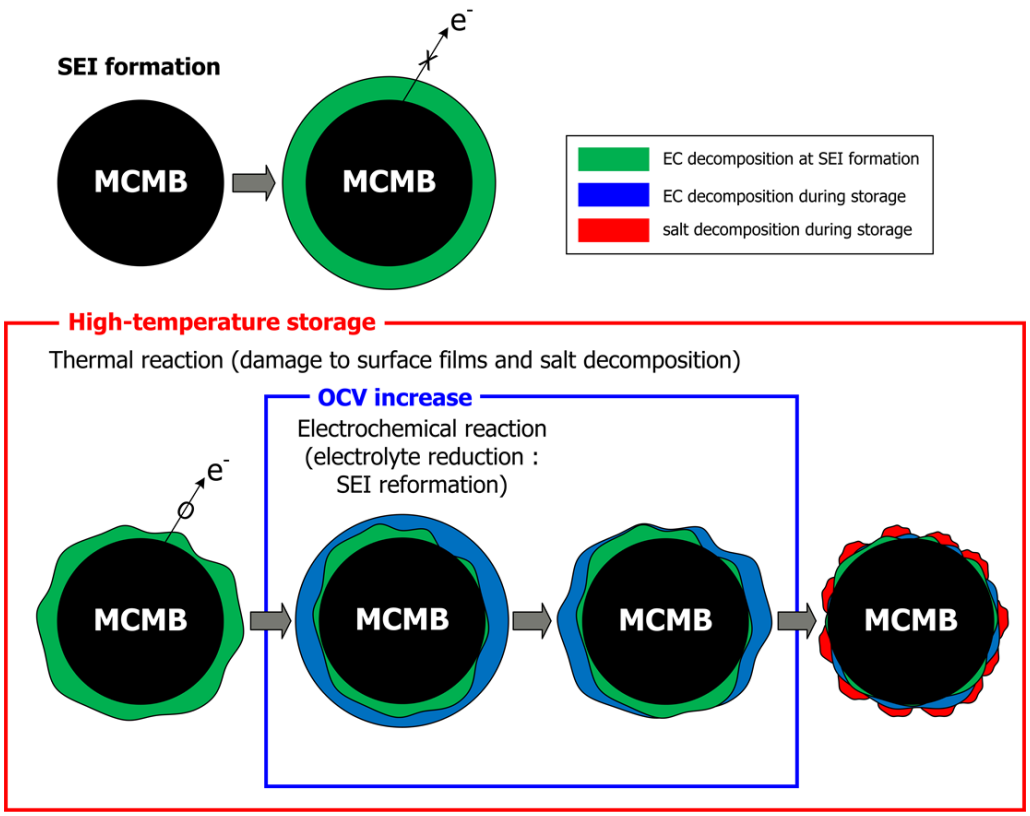

Figure 30. The schematic diagram of thermal behavior in the surface film.

passivating ability. Such a thermal degradation induces the increase of OCV value and the consumed electrons/lithium ions react with EC to repair the damaged surface film. The restored surface film can suppress the additional electrolyte decomposition in the sequent cycle right after high-temperature storage. Longer storage time, however, terminates continuous thermal reaction (thermal degradation) and electrochemical reaction (surface film regeneration) since the total amount of electrons/lithium ions are limited. After all, the surface film suffers from the thermal degradation dominantly. The graphite electrode surface is exposed and continuous decomposed products of lithium salt are deposited on the electrode surface. Namely, they lose their passivating ability, which causes the low Coulombic efficiency and large irreversible capacity in the sequent cycle right after high-temperature storage.

4.3. Comparative study on thermal stability of two SEI films derived electrolyte with different lithium salts

The surface film derived from $LiPF_6$-based electrolyte suffers thermal degradation in high-temperature storage at 85^{o}C. The damaged surface film loses its own passivating ability, one of the most essential requisites for SEI films. To enhance the thermal stability of surface films, many researches have been conducted. Typically, electrolyte additives, that is, SEI forming agents, are employed to modify the surface morphology or chemical composition in surface films. For example, vinylene carbonate (VC) is the most widely used electrolyte additive in the graphite negative electrode, which is easily

decomposed and polymerized to form thin and uniform surface layers [17,77,86-90]. Another approach is to vary solvents and lithium salts in the electrolyte solution. It is well known that the characteristics of surface films are influenced by not only electrolyte solvents but also lithium salts [29,74,81,91-93]. In this study, a comparative study on thermal stability of two SEI films derived electrolyte with different lithium salts is conducted.

Lithium bis(trifluoromethylsulfonyl)imide (LiTFSI) salt is well known to be more stable and safer than $LiPF_6$ salt [74,94]. It can be expected that the enhanced thermal stability of surface films would be derived from LiTFSI-containing electrolyte because of superior thermal stability of lithium salt itself [74]. After a pre-cycling, the galvanostatic charge/discharge voltages obtained in the initial two cycles are displayed in Fig. 31a. Totally identical voltage profiles in the first cycle are obtained from both electrolytes, which are typical shapes derived from the ethylene carbonate-based electrolyte solution. Fig. 31b compares the differential capacity (dQ/dV) plots that were derived from the galvanostatic charge/discharge voltage profiles. The dQ/dV profiles obtained in the initial two lithiation periods are represented. They also show similar dQ/dV profiles in both electrolytes. A reductive peak appears at 0.7 V (*vs.* Li/Li^+) in the first lithiation, but disappears in the second cycle. This peak is known to be associated with the reductive decomposition of carbonate-based organic electrolytes for SEI films on graphite electrodes [7,74]. Hence, the evolution of this peak in the first lithiation but the disappearance in the second lithiation illustrates that both SEI films, which forms in the first lithiation, passivates the graphite surface to prevent

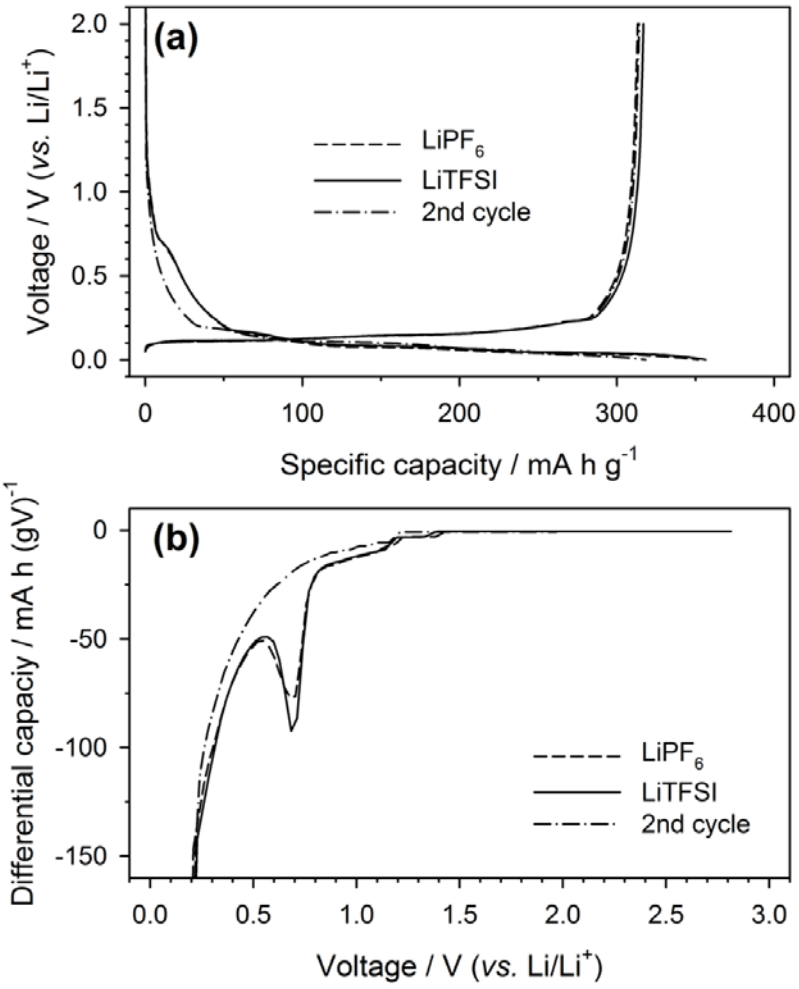

Figure 31. (a) The first and second galvanostatic charge/discharge voltage profiles of the Li/MCMB cells using either $LiPF_6$ or LiTFSI-based electrolyte obtained at 25°C. Specific current = 37.2 mA g^{-1}. Voltage cut-off range: 0.001~2 V. (b) Differential capacity (dQ/dV) plots derived from the above-represented voltage profiles.

additional electrolyte decomposition in the second cycle. As a result, the Coulombic efficiency, which is limited to 89% in the first cycle, becomes larger (*ca.* 98%) in the second cycle (Fig. 32). It is further noted that the Coulombic efficiency steadily increases to reach > 99% in the 5th cycle, ensuring that highly passivating surface films are generated in both electrolytes. Note that the high-temperature storage experiment was made at this point.

Fig. 33 compares the galvanostatic charge/discharge voltage profiles obtained in the initial two cycles and after storage at 85^{o}C, which were measured after a pre-cycling. On the voltage profile obtained in the $LiPF_6$-contatining electrolyte, the lithiation capacity starts to be delivered at 1.5 V (*vs.* Li/Li^+). The shoulder observed in the early lithiation region is much bigger than that in the first cycle. The voltage profile in the LITFSI-based electrolyte, however, is similar to that in the second cycle, where the SEI passivates the graphite surface to prevent additional electrolyte decomposition. Such behaviors can be observed noticeably in the dQ/dV plots (Fig. 34). On the dQ/dV profiles obtained in the $LiPF_6$-containing electrolyte, the 0.7 V peak reappears. The intensity of this peak is comparable to that appeared in the first lithiation before storage (Fig. 34a). These observations indicate that the SEI layer, which plays the passivation role before storage, is damaged during high-temperature storage to lose its passivating ability. As a result, the electrolyte decomposition is resumed to give a low Coulombic efficiency (85%) right after storage (Fig. 32). The dQ/dV plot shown in Fig. 34b, however, demonstrates a superior thermal stability for the SEI film generated from the LiTFSI-containing electrolyte. That is, the 0.7 V peak does not grow even after high-

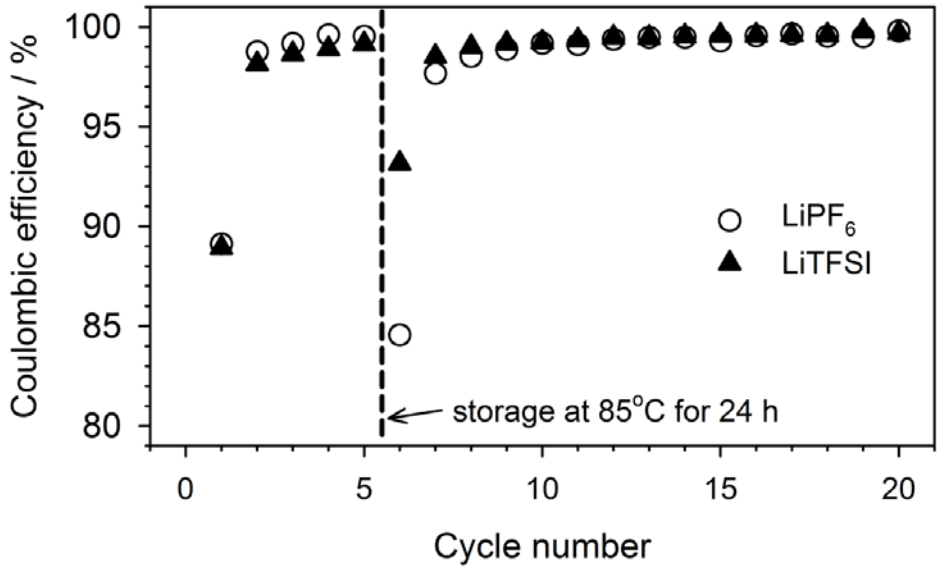

Figure 32. The Coulombic efficiency of Li/MCMB cells using either $LiPF_6$ or LiTFSI-based electrolyte before and after high-temperature storage at 85°C.

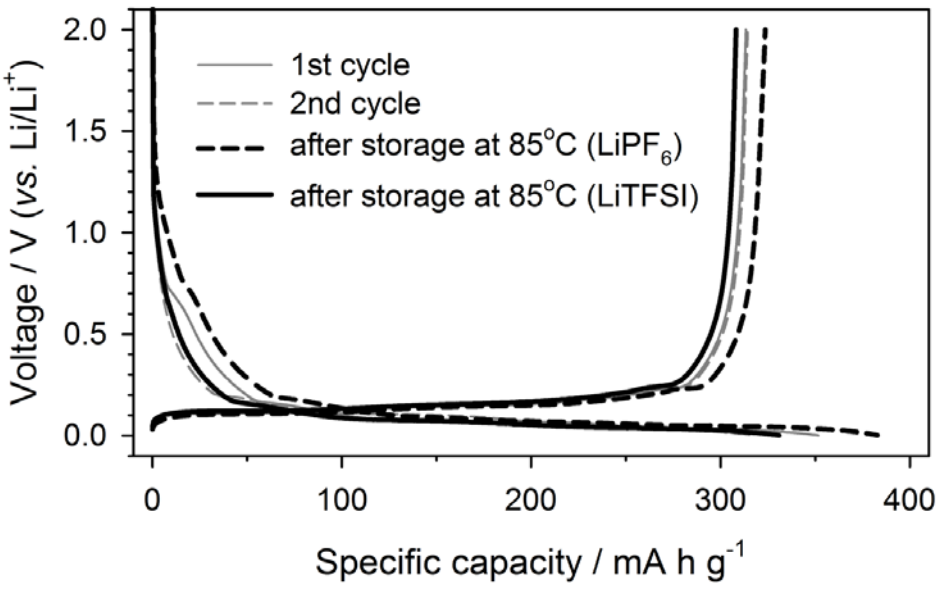

Figure 33. The galvanostatic charge/discharge voltage profiles of the Li/MCMB cells using either $LiPF_6$ or LiTFSI-based electrolyte, which are obtained at 25°C in the initial two cycles and after high-temperature storage at 85°C for 24 h. Specific current = 37.2 mA g^{-1}. Voltage cut-off range: 0.001~2 V.

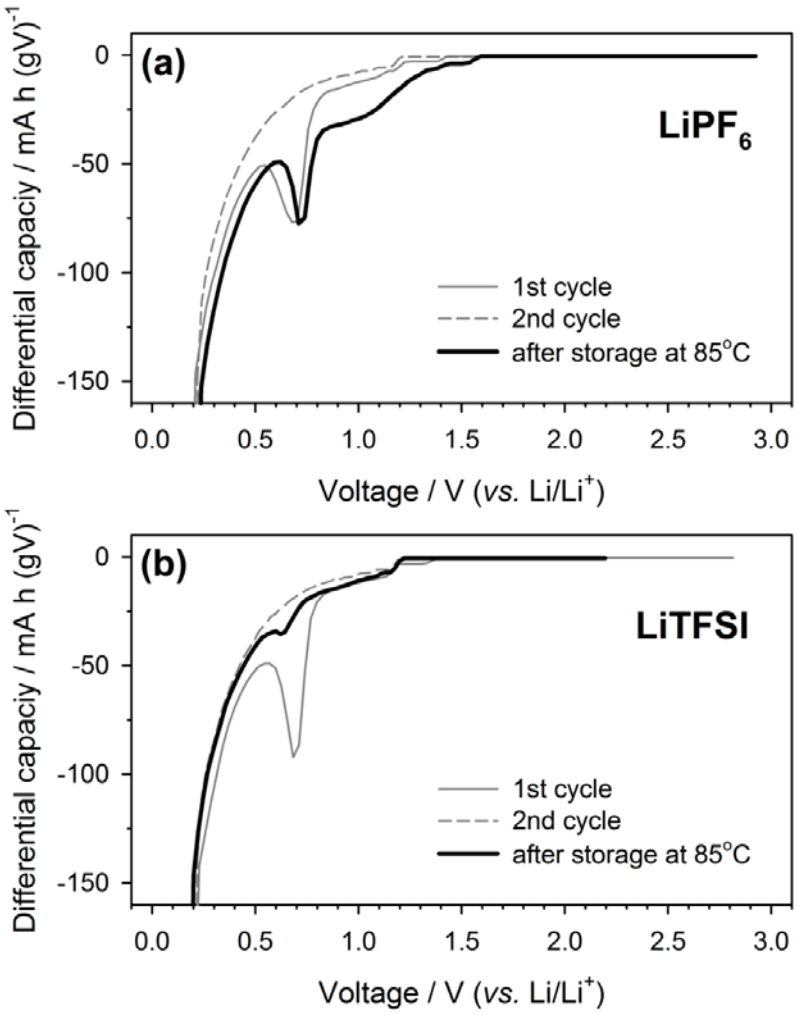

Figure 34. Differential capacity (dQ/dV) plots obtained in the initial two lithiation periods and after high-temperature storage at 85°C for 24 h. The galvanostatic charge/discharge was performed at 25°C, from which the dQ/dV profiles were derived: (a) in the $LiPF_6$ and (b) the LiTFSI-based electrolyte.

temperature storage, indicating that the electrolyte decomposition is only marginal, which in turn reflects that the SEI layer does not lose its passivating ability even after high-temperature exposure. The higher Coulombic efficiency (93%) obtained right after storage (Fig. 32) ensures the higher passivating ability and thus a superior thermal stability of this surface film.

The loss of passivating ability due to thermal degradation is further confirmed by monitoring the OCV value during high-temperature storage. Fig. 35 displays the OCV variation upon a temperature ramp from 25^{o}C to 120^{o}C. In both electrolytes, the OCV remains at the initial value (*ca.* 1.5 V *vs.* Li/Li^{+}) until 60^{o}C. However, the OCV starts to increase from 60^{o}C to reach each limiting value. The OCV increase is a signature for the oxidation of graphite electrode, during which Li^{+} ions and the equivalent amount of electrons are transferred from the graphite electrode to the electrolyte at the interface (de-lithiation reaction). Such a charge transfer is impossible if SEI layers are perfectly passivating. Hence, the OCV increase is an indication of a loss of passivating ability, which has resulted from thermal degradation of surface films. The OCV profiles in Fig. 35 illustrate that two SEI layers are passivating until 60^{o}C, but lose the passivating ability from 60^{o}C. This reflects that the SEI layers are not thermally degraded until 60^{o}C, but the thermal damage starts from 60^{o}C. The extent of thermal damage can be assessed from the OCV profiles in Fig. 35. In the $LiPF_6$-based electrolyte, the OCV increases up to 3.0 V, which is the value for the fully de-lithiated graphite (x = 0 in Li_xC_6), demonstrating that all of Li^{+} ions/electrons are transferred from the graphite electrode to the electrolyte due to the poor passivating ability of the damaged SEI layer.

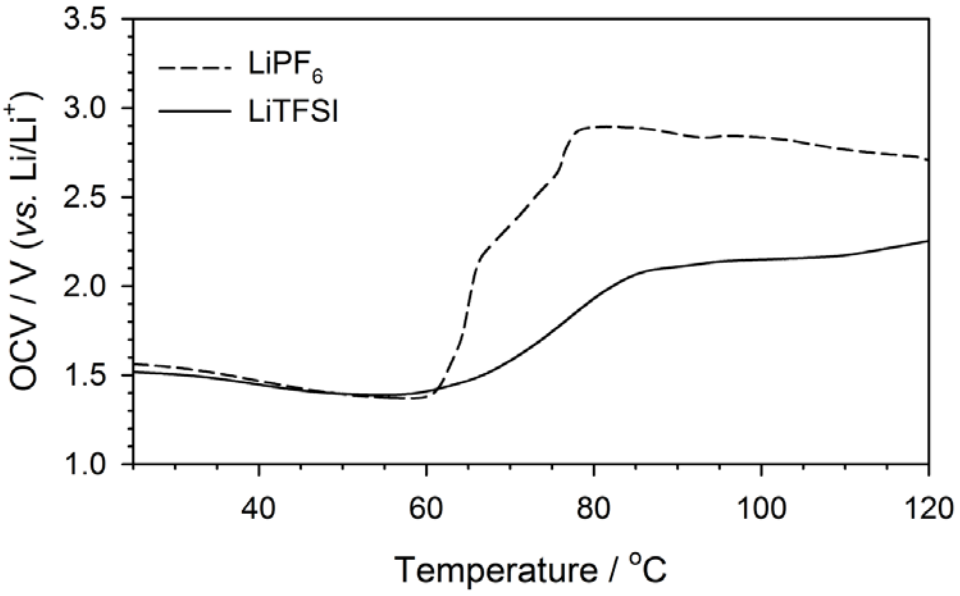

Figure 35. The variation of open-circuit voltage (OCV) of the Li/MCMB cells using either $LiPF_6$ or LiTFSI-based electrolyte during high-temperature storage with a temperature sweep from 25°C to 120°C at a ramp rate of 0.1°C min^{-1}.

However, the final OCV is *ca.* 2.0 V in the LiTFSI-containing electrolyte, suggesting that the charge (Li^+ ions/electrons) transfer is less significant since the SEI layer is still passivating. Fig. 36a displays the OCV change traced at 55°C, where two SEI films are expectedly intact as suggested in Fig. 35. As expected, the OCV change is negligible, ensuring that both SEI films are intact and thus still passivating (Fig. 36a). The OCV measurement was also performed at 85°C, where serious film degradation is expected from the profiles shown in Fig. 35. As expected, the OCV increases in both electrolytes; up to 3.0 V in the $LiPF_6$-based electrolyte and 2.0 V in the LiTFSI-based electrolyte, respectively (Fig. 36b). In short, the SEI film generated from the LiTFSI-based electrolyte (LiTFSI-surface film, hereafter) is less damaged due to superior thermal stability.

The most convincing evidence for SEI degradation may be found on the SEM images taken after high-temperature storage. Fig. 37 displays the SEM image of pristine electrode surface, in which the MCMB (the larger particles) and Super P (the smaller particles) are bound by the PVdF binder. After a pre-cycling (five cycles at 25°C before the high-temperature storage), the foreign materials are deposited on the electrode surfaces, which must be the SEI films deposited by electrolyte decomposition. The SEI layers derived from two electrolytes effectively cover the electrode surfaces (Figs. 37b and 37d). One notable difference between two films is, however, the presence of cracks or void spaces in the film generated from the $LiPF_6$-based electrolyte (Fig. 37b, $LiPF_6$-surface film, hereafter). After storage, two surface films show a big morphological difference. $LiPF_6$-surface film is now converted into a rough

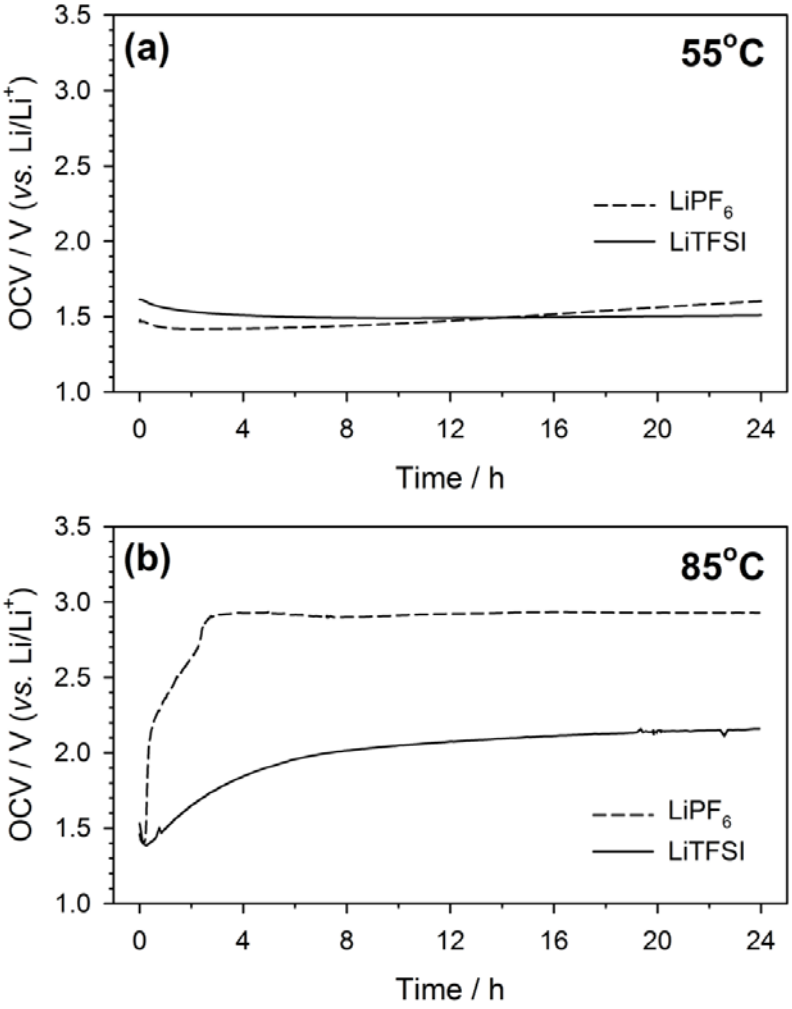

Figure 36. The variation of open-circuit voltage (OCV) of the Li/MCMB cells using either $LiPF_6$ or LiTFSI-based electrolyte during high-temperature storage fixed at (a) 55°C and (b) 85°C.

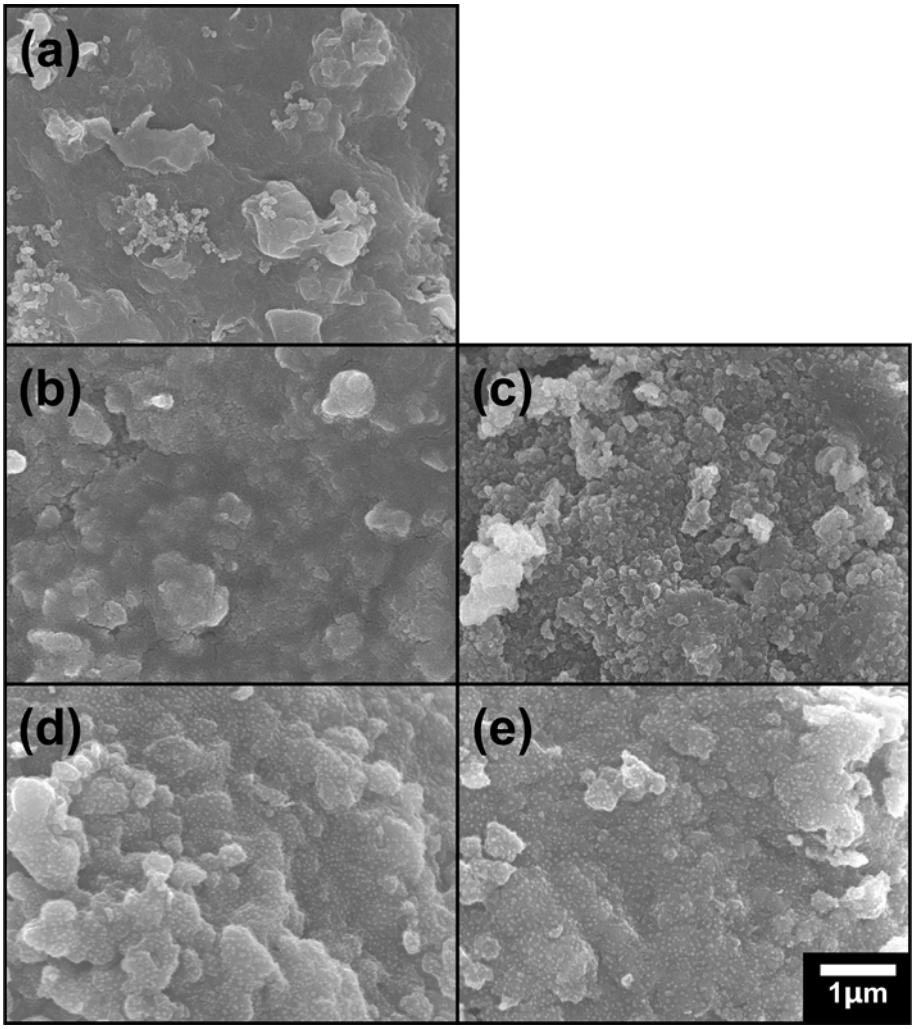

Figure 37. FE-SEM images taken on the surface MCMB electrodes: (a) pristine, (b)/(d) before storage (after a pre-cycling), and (c)/(e) after high-temperature storage at 85^{o}C for 24 h. Note that $LiPF_6$-surface film/LiTFSI-surface film in order.

and unevenly covered one (Fig. 37c), whereas LiTFSI-surface film largely maintains its initial morphology (Figs. 37d and 37e). Evidently, the former is severely damaged, whereas the latter is rather intact. This is what is observed in the dQ/dV plots (Fig. 36) and the OCV measurement.

The results presented so far consistently demonstrate a superior thermal stability of LiTFSI-surface film. To gain an insight into the factors affecting the thermal stability of SEI films, the film compositions are analyzed by using XPS (Figs. 38 and 39). At a glance, there appears a notable change on the X-ray photoelectron spectra taken on $LiPF_6$-surface film after storage (Fig. 38), but the change is only marginal for LiTFSI-surface film (Fig. 39). The insignificant compositional change in LiTFSI-surface film again ascertains the robustness of this film for thermal degradation. To address how the chemical composition has an effect on the thermal stability of surface films, the XPS data taken before storage are analyzed. A comparison made for the C 1s spectra taken before storage reveals that the population of carbon-oxygen species ($ROCO_2Li$ or Li_2CO_3 at 290.3 eV and O=C-O at 289 eV) is larger for LiTFSI-surface film (Fig. 39a). This feature is further confirmed on the O 1s spectra. As seen, LiTFSI-surface film gives rise to a higher intensity for the carbon-oxygen species at 532 eV and 533.5 eV (Fig. 39b). The high population of carbon-oxygen species in LiTFSI-surface film is contrasted by the high population of the F-containing species in $LiPF_6$-surface film. Notably, the population of LiF is dominant over the other F-species in $LiPF_6$-surface film (Fig. 38c). The relative atomic concentration for four elements (O, C, F and Li) was calculated from the XPS data and displayed in Fig. 40 and Table 2. Before the

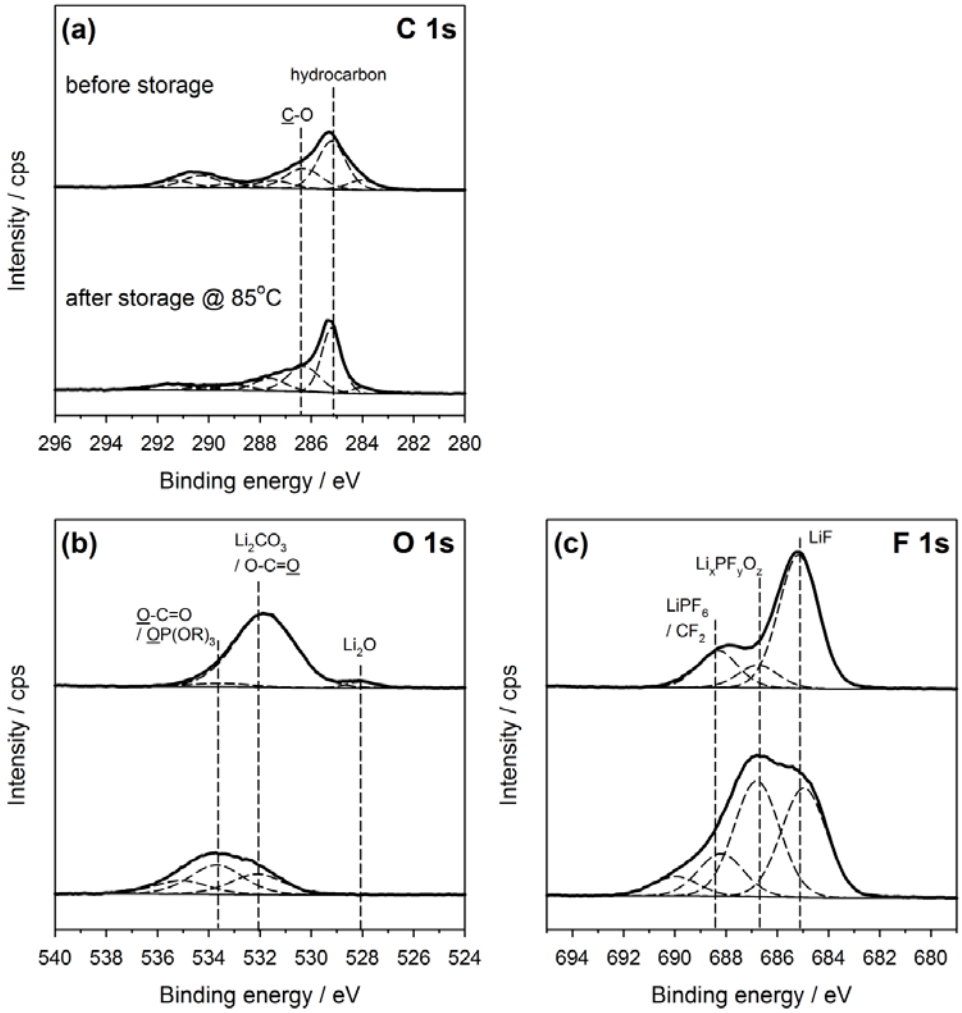

Figure 38. (a) C 1s, (b) O 1s, and (c) F 1s XPS spectra obtained from the MCMB electrodes using the $LiPF_6$-based electrolyte before and after high-temperature storage at 85°C for 24 h.

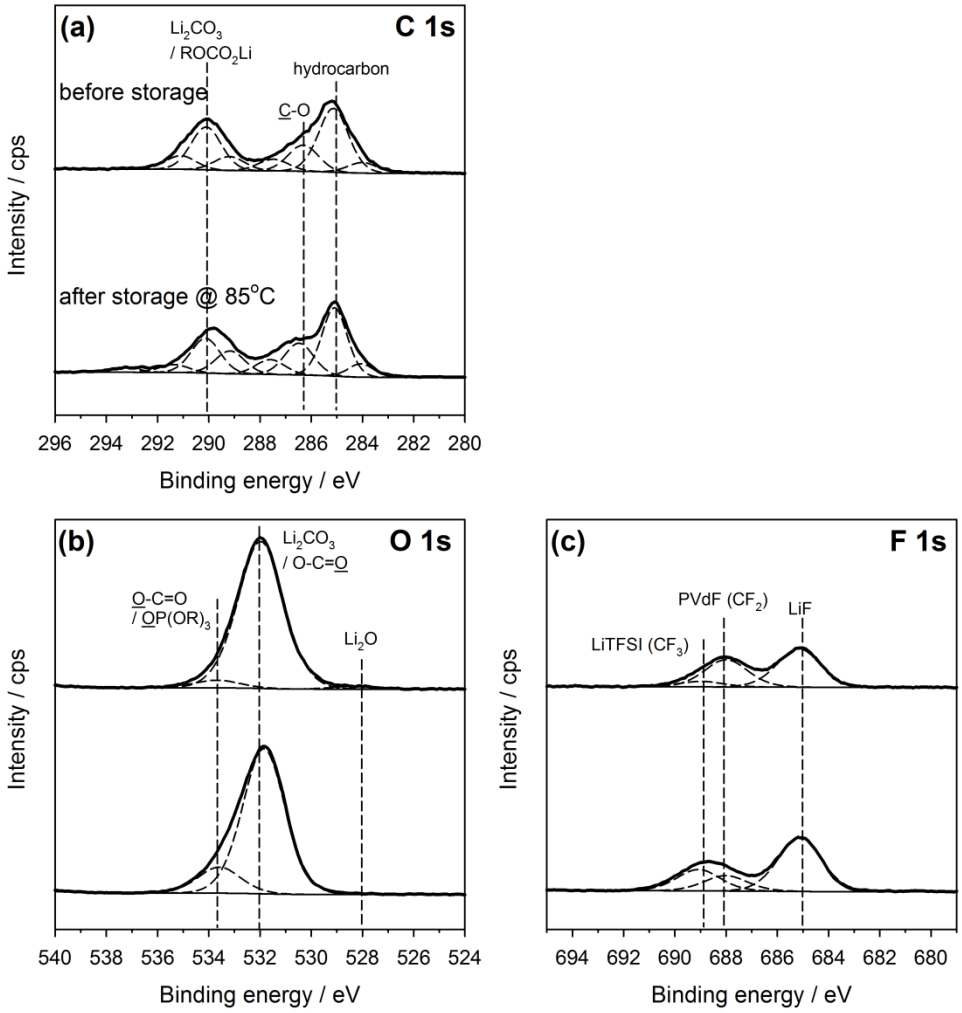

Figure 39. (a) C 1s, (b) O 1s, and (c) F 1s XPS spectra obtained from the MCMB electrodes using the LiTFSI-based electrolyte before and after high-temperature storage at 85°C for 24 h.

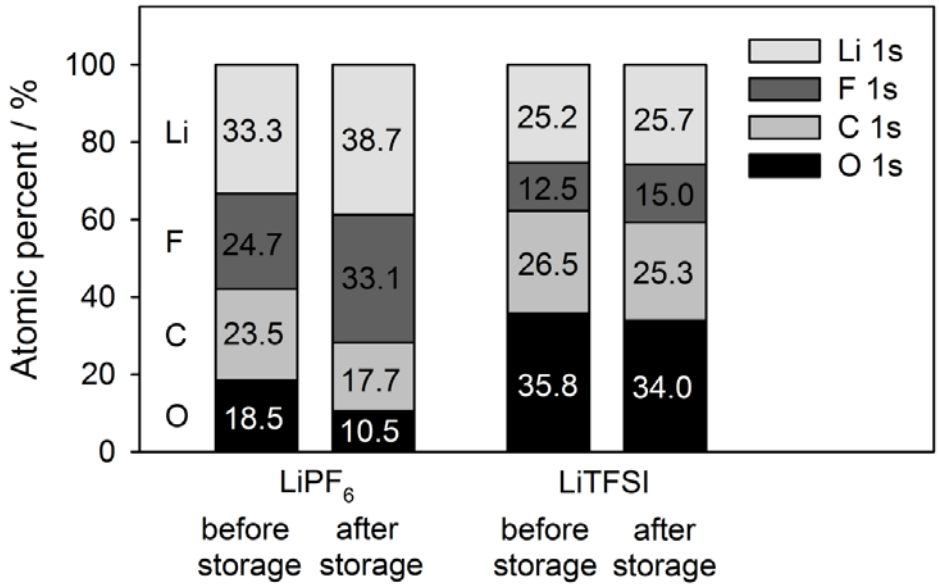

Figure 40. Atomic composition in the surface films, which was calculated from the XPS data obtained before and after storage at 85°C for 24 h in either $LiPF_6$ or LiTFSI-surface film.

Table 2. Atomic concentration of each element obtained from XPS spectra of the graphite negative electrode using either $LiPF_6$ or LiTFSI-based electrolyte before and after high-temperature storage at 85°C.

Element	$LiPF_6$-surface film (%)		LiTFSI-surface film (%)	
	before storage	after storage	before storage	after storage
Li 1s	33.3	38.7	25.2	25.7
F 1s	24.7	33.1	12.5	15.0
C 1s	23.5	17.7	26.5	25.3
O 1s	18.5	10.5	35.8	34.0

storage, the Li- and F-containing species are enriched in $LiPF_6$-surface film, whereas the population of organic carbon-oxygen species is higher in LiTFSI-surface film. The carbon-oxygen species must come from the organic carbonate solvents (EC and DEC in this work), whereas the F-species must come from the lithium salts; $LiPF_6$ and LiTFSI, respectively. The higher population of inorganic F-species ($LiPF_6$, $Li_xPF_yO_z$, and LiF) in $LiPF_6$-surface film implies that $LiPF_6$ decomposes during the initial SEI formation period along with a reductive decomposition of carbonate solvents. It is known that $LiPF_6$ is readily decomposed into LiF(s) and PF_5(g), and also hydrolyzed by impurity water to generate hydrofluoric acid (HF) [95-97]. HF can further induce the LiF formation [14,98,99]. Meanwhile, the lithium salt in the LiTFSI-based electrolyte is LiTFSI that carries $-CF_3$ moiety. It is likely that $-CF_3$ moiety is not easily decomposed due to strong C-F bond. As expected, the population of F-species in LiTFSI-surface film (12.5%) is only one-half of that (24.7%) found in $LiPF_6$-surface film.

The results so far reveal the difference in chemical composition and film morphology between two surface films. $LiPF_6$-surface film, which shows a poorer thermally stability, is enriched by the inorganic Li- and F-species that are generated from $LiPF_6$. This film carries the cracks or void spaces. In contrast, thermally more stable LiTFSI-surface film is enriched by the carbon-oxygen species that are generated from the organic carbonate solvents (EC and DEC in this study). This film fully covers the electrode surface. Evidently, the organic-rich surface film with uniform coverage seems to be favored for thermal stability. However, the underlying relationships

between the film composition/morphology and thermal stability cannot be identified at this point. In short, a severe damage is observed in $LiPF_6$-surface film upon storage. Also, the increase of Li- and F-species at the expense of the carbon-oxygen species is noted after storage. The unevenly covered surface film that is even more enriched by the Li- and F-species seems to have a poorer passivating ability. As a result, the dQ/dV plot traced after storage shows a strong electrolyte reduction current, and the Coulombic efficiency is low (85%) right after storage. In contrast, LiTFSI-surface film is relatively intact in its morphology upon the high-temperature storage. Also, the compositional change is only marginal. As a result, the film does not lose its initial passivating ability. However, the slight compositional change reflects that this film is not perfectly intact upon the high-temperature storage.

To be extensive study on superior thermal stability of LiTFSI-surface film, the MCMB electrodes are prepared with various SOC states and the OCV measurements during storage at 85^{o}C are conducted. Fig. 41 shows the variation of OCV upon storage time, of which behavior is totally different from that in $LiPF_6$-based electrolyte (Fig. 16). The OCV value increases upon storage time as well; however, the extent of increase is very small. Consumed capacity can be calculated by recycling at 25^{o}C after storage (Fig. 42). Compared to that in the $LiPF_6$-based electrolyte, the consumed capacity during storage at 85^{o}C is reduced remarkably thanks to superior thermal stability of LiTFSI-surface film (Fig. 43). One notable distinction in here is that the consumption of electrons/lithium ions is quantitatively small even in the highly reductive condition (SOC100). The consumed capacity during storage is irreversible,

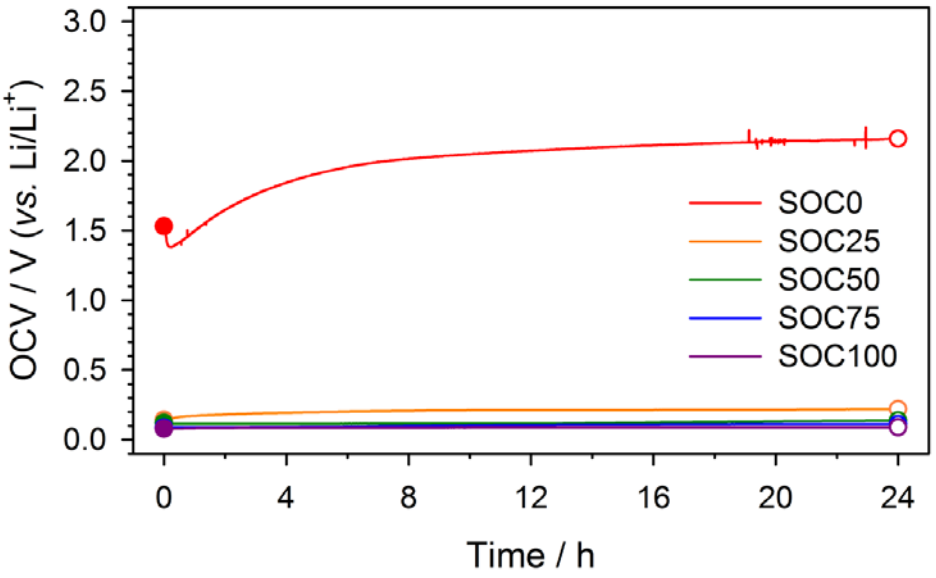

Figure 41. The variation of open-circuit voltage (OCV) of the Li/MCMB cell using the LiTFSI-based electrolyte during high-temperature storage at 85°C.

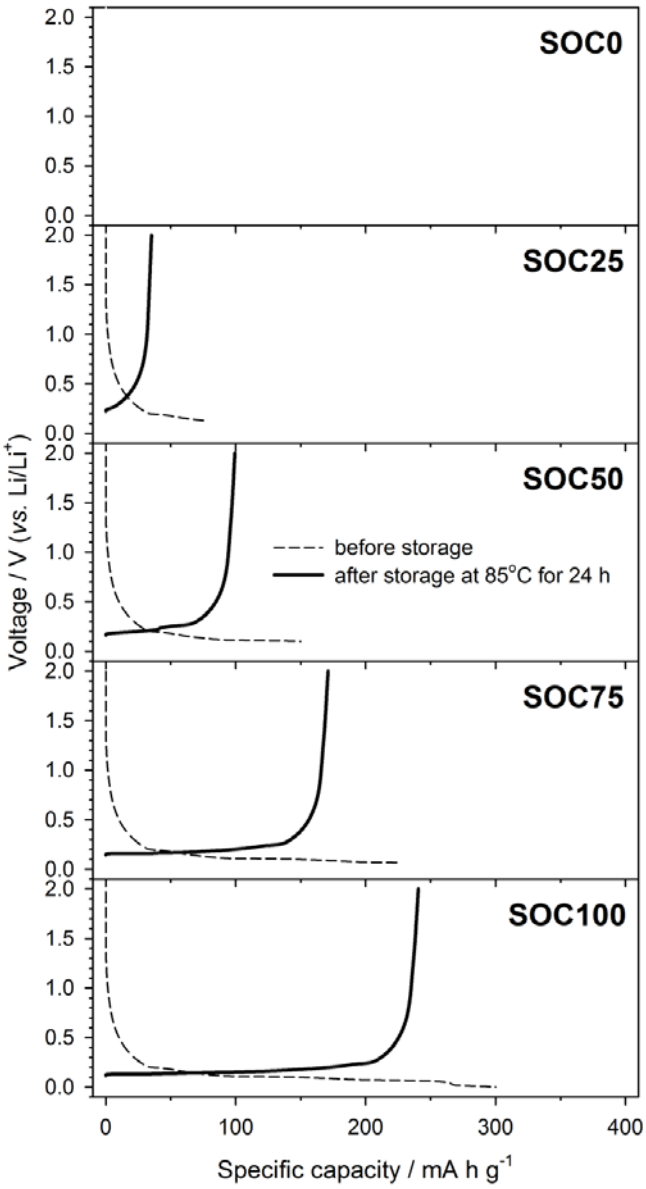

Figure 42. The galvanostatic charge/discharge voltage profiles of Li/MCMB cells using the LiTFSI-based electrolyte before (dash line) and after (solid line) high-temperature storage at 85°C for 24 h.

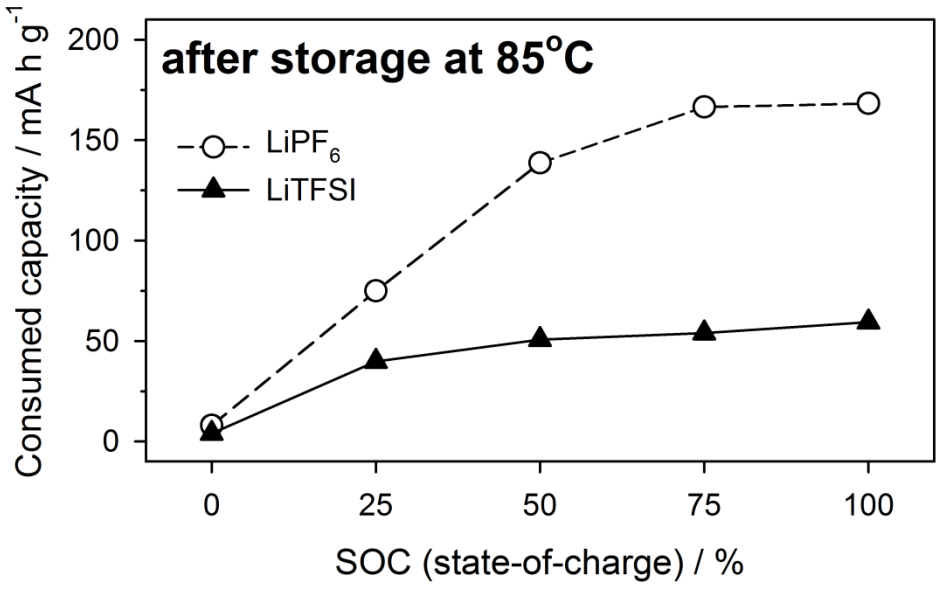

Figure 43. Consumed capacity of Li/MCMB cells cells using either $LiPF_6$ or LiTFSI-based electrolyte during high-temperature storage at 85°C for 24h.

which is used to repair the thermally damaged surface film. Therefore, superior thermal stability of surface film can contribute to enhance cycle life in the case of the full-cell system. After storage at 85^{o}C, LiTFSI-surface film in all the SOC states keeps its passivating ability (Fig. 44). In short, it is ascertained that thermal stability of surface film derived from LiTFSI-based electrolyte is superior regardless of SOC states in the graphite negative electrode.

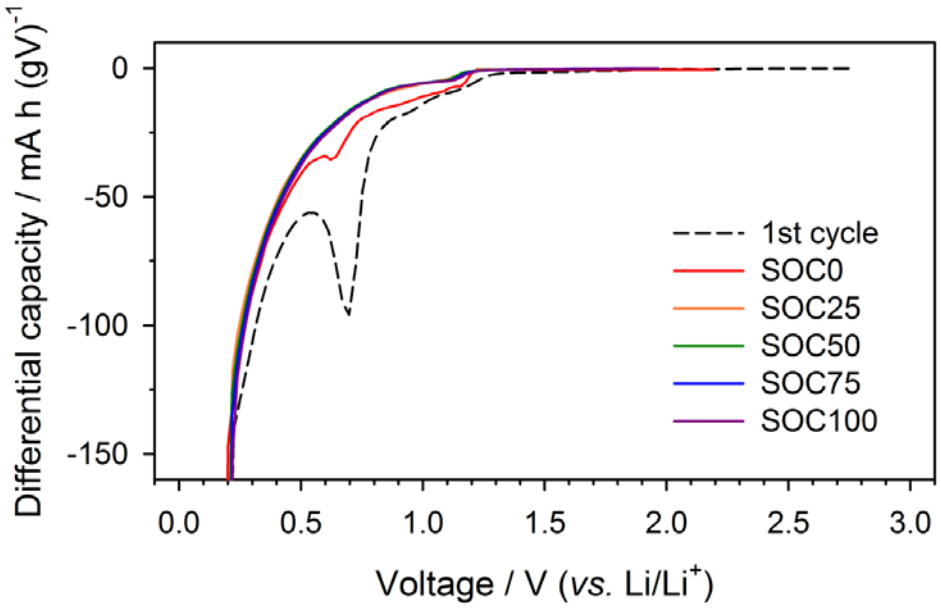

Figure 44. Differential capacity (dQ/dV) plots of the Li/MCMB cells using LiTFSI-based electrolyte in the first lithiation period and after high-temperature storage at 85^{o}C for 24 h. The galvanostatic charge/discharge was performed at 25^{o}C, from which the dQ/dV profiles were derived.

5. Conclusions

In this work, thermal stability and thermal behavior of surface films derived from the conventional $LiPF_6$-based electrolyte on graphite negative electrode is investigated. Firstly, thermal stability of surface film is evaluated using the OCV measurements during high-temperature storage either with temperature ramp or at fixed temperature. Secondly, the mechanism of thermal behavior of surface films is elucidated by controlling SOC of graphite electrode and storage time. Finally, thermal stability of two surface films is compared, from which the factors controlling the thermal stability has been delineated. The following points of value are summarized.

(i) The OCV measurement is effectively used to assess the passivating ability of surface films during high-temperature storage. The increase of OCV value means loss of electron from the graphite negative electrode since thermal degradation of surface film loses its own passivating ability as an electrical insulator. The OCV of graphite electrode remains at the initial value until 60^oC since the films are intact to maintain their initial passivating ability. The OCV increases from 60^oC due to the loss of passivating ability. During high-temperature storage at 85^oC, the OCV increases dramatically just in short time, that indicates the surface films derive from $LiPF_6$-baed electrolyte are thermally unstable.

(ii) The thermal behavior of surface films turns out to be determined by two conflicting reactions during high-temperature storage; thermal reaction and electrochemical reaction. Thermal degradation of surface films preferentially starts to

occur, and it provokes exposure of graphite electrode surface and the loss of passivating ability of surface films throughout the high-temperature storage. And also, $LiPF_6$ salt is thermally decomposed to deposit on the damaged films. Meanwhile, consumed electrons and lithium ions can electrochemically react with ethylene carbonate to repair the thermally damaged surface films, of which the surface morphology and chemical composition resemble those of original SEI films. The regenerated surface films can plays a good passivating role after the high-temperature storage. In short, the thermal reaction preferentially contributes to the thermal behavior of surface films by thermal degradation; however, the electrochemical reaction is dominant until electrons and lithium ions in the graphite negative electrode are consumed utterly.

(iii) The SEI films that are enriched by Li- or F-containing inorganic species turn out to be thermally less stable. Cracks or void spaces are also found on this surface film. On the contrary, the SEI film, which is enriched by the organic carbon-oxygen species, uniformly covers the graphite surface. It appears that the film composition and morphology does not change even upon a high-temperature exposure and the passivating ability is still functional. The factors controlling the thermal stability of surface films appear to be the chemical composition and film morphology. The organic-rich and uniformly covered surface films are favored for thermal stability.

References

1. J. M. Tarascon and M. Armand, *Nature*, **414**, 359 (2001).
2. M. D. Levi, C. Wang, J. S. Gnanaraj and D. Aurbach, *J. Power Sources*, **119–121**, 538 (2003).
3. J. R. Dahn, T. Zheng, Y. Liu and J. S. Xue, *Science*, **270**, 590 (1995).
4. Z. X. Shu, R. S. McMillan and J. J. Murray, *J. Electrochem. Soc.*, **140**, 922 (1993).
5. R. Fong, U. von Sacken and J. R. Dahn, *J. Electrochem. Soc.*, **137**, 2009 (1990).
6. E. Peled, *J. Electrochem. Soc.*, **126**, 2047 (1979).
7. J. O. Besenhard, M. Winter, J. Yang and W. Biberacher, *J. Power Sources*, **54**, 228 (1995).
8. E. Peled, D. Golodnitsky, C. Menachem and D. Bar-Tow, *J. Electrochem. Soc.*, **145**, 3482 (1998).
9. A. S. Claye, J. E. Fischer, C. B. Huffman, A. G. Rinzler and R. E. Smalley, *J. Electrochem. Soc.*, **147**, 2845 (2000).
10. K. Kanamura, H. Tamura, S. Shiraishi and Z.-i. Takehara, *J. Electrochem. Soc.*, **142**, 340 (1995).
11. J. Yamaki, in *Encyclopedia of Electrochemical Power Sources*, G. Jürgen, Editor, p. 183, Elsevier, Amsterdam (2009).
12. A. M. Andersson and K. Edström, *J. Electrochem. Soc.*, **148**, A1100 (2001).
13. K. Araki and N. Sato, *J. Power Sources*, **124**, 124 (2003).
14. K. Tasaki, A. Goldberg, J.-J. Lian, M. Walker, A. Timmons and S. J. Harris, *J.*

Electrochem. Soc., **156**, A1019 (2009).

15. Y. Reynier, R. Yazami and B. Fultz, in *Battery Conference on Applications and Advances, 2002. The Seventeenth Annual*, p. 145 (2002).

16. R. Yazami and Y. F. Reynier, *Electrochim. Acta*, **47**, 1217 (2002).

17. M. Inaba, H. Tomiyasu, A. Tasaka, S.-K. Jeong and Z. Ogumi, *Langmuir*, **20**, 1348 (2004).

18. W. Li, A. Xiao, B. L. Lucht, M. C. Smart and B. V. Ratnakumar, *J. Electrochem. Soc.*, **155**, A648 (2008).

19. M. Winter, *Z. Phys. Chem.*, **223**, 1395 (2009).

20. L. Bodenes, R. Dedryvère, H. Martinez, F. Fischer, C. Tessier and J.-P. Pérès, *J. Electrochem. Soc.*, **159**, A1739 (2012).

21. S.-i. Tobishima, K. Takei, Y. Sakurai and J.-i. Yamaki, *J. Power Sources*, **90**, 188 (2000).

22. S.-i. Tobishima and J.-i. Yamaki, *J. Power Sources*, **81-82**, 882 (1999).

23. M. N. Richard and J. R. Dahn, *J. Electrochem. Soc.*, **146**, 2068 (1999).

24. A. M. Andersson, M. Herstedt, A. G. Bishop and K. Edström, *Electrochim. Acta*, **47**, 1885 (2002).

25. J.-i. Yamaki, H. Takatsuji, T. Kawamura and M. Egashira, *Solid State Ionics*, **148**, 241 (2002).

26. E.-S. Hong, S. Okada, T. Sonoda, S. Gopukumar and J.-i. Yamaki, *J. Electrochem. Soc.*, **151**, A1836 (2004).

27. A. Xiao, L. Yang, B. L. Lucht, S.-H. Kang and D. P. Abraham, *J. Electrochem. Soc.*,

156, A318 (2009).

28. D. Ensling, M. Stjerndahl, A. Nytén, T. Gustafsson and J. O. Thomas, *J. Mater. Chem.*, **19**, 82 (2009).

29. S. Leroy, H. Martinez, R. Dedryvère, D. Lemordant and D. Gonbeau, *Appl. Surf. Sci.*, **253**, 4895 (2007).

30. K. Nishio, in *Encyclopedia of Electrochemical Power Sources*, G. Jürgen, Editor, p. 68, Elsevier, Amsterdam (2009).

31. M. S. Whittingham, *Chem. Rev.*, **104**, 4271 (2004).

32. J. O. Besenhard and H. P. Fritz, *Journal of Electroanalytical Chemistry and Interfacial Electrochemistry*, **53**, 329 (1974).

33. J. O. Besenhard and G. Eichinger, *Journal of Electroanalytical Chemistry and Interfacial Electrochemistry*, **68**, 1 (1976).

34. G. Eichinger and J. O. Besenhard, *Journal of Electroanalytical Chemistry and Interfacial Electrochemistry*, **72**, 1 (1976).

35. K. Mizushima, P. C. Jones, P. J. Wiseman and J. B. Goodenough, *Materials Research Bulletin*, **15**, 783 (1980).

36. K. Mizushima, P. C. Jones, P. J. Wiseman and J. B. Goodenough, *Solid State Ionics*, **3–4**, 171 (1981).

37. M. Winter, J. O. Besenhard, M. E. Spahr and P. Novák, *Adv. Mater.*, **10**, 725 (1998).

38. M. B. Armand, in *Materials for Advanced Batteries*, D. W. M. J. B. B. C. H. Steele, Editor, p. 145, Plenum, New York (1980).

39. T. Ohzuku, Y. Iwakoshi and K. Sawai, *J. Electrochem. Soc.*, **140**, 2490 (1993).

40. J. O. Besenhard and H. P. Fritz, *Angewandte Chemie International Edition in English*, **22**, 950 (1983).

41. L. B. Ebert, *Annual Review of Materials Science*, **6**, 181 (1976).

42. R. E. Franklin, *Proceedings of the Royal Society of London. Series A. Mathematical and Physical Sciences*, **209**, 196 (1951).

43. J. R. Dahn, W. Xing and Y. Gao, *Carbon*, **35**, 825 (1997).

44. R. Alcántara, J. M. Jiménez Mateos and J. L. Tirado *J. Electrochem. Soc.*, **149**, A201 (2002).

45. A. N. Dey, *J. Electrochem. Soc.*, **118**, 1547 (1971).

46. R. A. Huggins, *J. Power Sources*, **81–82**, 13 (1999).

47. M. Winter and J. O. Besenhard, *Electrochim. Acta*, **45**, 31 (1999).

48. J. Y. Kwon, J. H. Ryu and S. M. Oh, *Electrochim. Acta*, **55**, 8051 (2010).

49. U. Kasavajjula, C. Wang and A. J. Appleby, *J. Power Sources*, **163**, 1003 (2007).

50. G. Taillades, N. Benjelloun, J. Sarradin and M. Ribes, *Solid State Ionics*, **152–153**, 119 (2002).

51. N.-S. Choi, K. H. Yew, K. Y. Lee, M. Sung, H. Kim and S.-S. Kim, *J. Power Sources*, **161**, 1254 (2006).

52. J. N. Reimers and J. R. Dahn, *J. Electrochem. Soc.*, **139**, 2091 (1992).

53. J. N. Reimers, J. R. Dahn and U. von Sacken, *J. Electrochem. Soc.*, **140**, 2752 (1993).

54. K. Mizushima, P. C. Jones, P. J. Wiseman and J. B. Goodenough, *Materials Research Bulletin*, **15**, 783 (1980).

55. A. Mendiboure, C. Delmas and P. Hagenmuller, *Materials Research Bulletin*, **19**, 1383 (1984).

56. J. Cho, Y. J. Kim, T.-J. Kim and B. Park, *Angew. Chem. Int. Ed.*, **40**, 3367 (2001).

57. S. A. Campbell, C. Bowes and R. S. McMillan, *Journal of Electroanalytical Chemistry and Interfacial Electrochemistry*, **284**, 195 (1990).

58. Y. Nitta, K. Okamura, K. Haraguchi, S. Kobayashi and A. Ohata, *J. Power Sources*, **54**, 511 (1995).

59. T. Ohzuku, A. Ueda and M. Kouguchi, *J. Electrochem. Soc.*, **142**, 4033 (1995).

60. J. Cho, T.-J. Kim, Y. J. Kim and B. Park, *Electrochem. Solid-State Lett.*, **4**, A159 (2001).

61. M. M. Thackeray, P. J. Johnson, L. A. de Picciotto, P. G. Bruce and J. B. Goodenough, *Materials Research Bulletin*, **19**, 179 (1984).

62. T. Ohzuku, M. Kitagawa and T. Hirai, *J. Electrochem. Soc.*, **137**, 769 (1990).

63. R. J. Gummow, A. de Kock and M. M. Thackeray, *Solid State Ionics*, **69**, 59 (1994).

64. D. H. Jang and S. M. Oh, *J. Electrochem. Soc.*, **144**, 3342 (1997).

65. J. M. Tarascon, E. Wang, F. K. Shokoohi, W. R. McKinnon and S. Colson, *J. Electrochem. Soc.*, **138**, 2859 (1991).

66. L. Guohua, H. Ikuta, T. Uchida and M. Wakihara, *J. Electrochem. Soc.*, **143**, 178 (1996).

67. A. M. Kannan and A. Manthiram, *Electrochem. Solid-State Lett.*, **5**, A167 (2002).

68. S. Lim and J. Cho, *Electrochem. Commun.*, **10**, 1478 (2008).

69. G.-W. Lee, J.-H. Lee, J. H. Ryu and S. M. Oh, *J. Korean Electrochem. Soc.*, **12**, 81

(2009).

70. A. K. Padhi, K. S. Nanjundaswamy and J. B. Goodenough, *J. Electrochem. Soc.*, **144**, 1188 (1997).

71. D. Morgan, A. Van der Ven and G. Ceder, *Electrochem. Solid-State Lett.*, **7**, A30 (2004).

72. S.-Y. Chung, J. T. Bloking and Y.-M. Chiang, *Nat Mater*, **1**, 123 (2002).

73. V. Srinivasan and J. Newman, *J. Electrochem. Soc.*, **151**, A1517 (2004).

74. K. Xu, *Chem. Rev.*, **104**, 4303 (2004).

75. A. Chagnes and J. Swiatowska, Electrolyte and Solid-Electrolyte Interphase Layer in Lithium-Ion Batteries, in *Lithium Ion Batteries - New Developments*, I. Belharouak Editor, p. 145, InTech (2012).

76. R. McMillan, H. Slegr, Z. X. Shu and W. Wang, *J. Power Sources*, **81-82**, 20 (1999).

77. D. Aurbach, K. Gamolsky, B. Markovsky, Y. Gofer, M. Schmidt and U. Heider, *Electrochim. Acta*, **47**, 1423 (2002).

78. J. F. Moulder, W. F. Stickle, P. E. Sobol and K. D. Bomben, *Handbook of X Ray Photoelectron Spectroscopy: A Reference Book of Standard Spectra for Identification and Interpretation of Xps Data*, Physical Electronics, Inc., Eden Prairie, Minnesota (1995).

79. D. Aurbach, Y. Gofer, M. Ben-Zion and P. Aped, *J. Electroanal. Chem.*, **339**, 451 (1992).

80. K. Xu and A. von Cresce, *J. Mater. Chem.*, **21**, 9849 (2011).

81. H. Park, T. Yoon, J. Mun, J. H. Ryu, J. J. Kim and S. M. Oh, *J. Electrochem. Soc.*, **160**, A1539 (2013).

82. S. Park, J. H. Ryu and S. M. Oh, *J. Korean Electrochem. Soc.*, **15**, 19 (2012).

83. L. El Ouatani, R. Dedryvère, J.-B. Ledeuil, C. Siret, P. Biensan, J. Desbrières and D. Gonbeau, *J. Power Sources*, **189**, 72 (2009).

84. R. Dedryvère, L. Gireaud, S. Grugeon, S. Laruelle, J.-M. Tarascon and D. Gonbeau, *J. Phys. Chem. B*, **109**, 15868 (2005).

85. S. E. Sloop, J. K. Pugh, S. Wang, J. B. Kerr and K. Kinoshita, *Electrochem. Solid-State Lett.*, **4**, A42 (2001).

86. S. Park, J. H. Ryu and S. M. Oh, *J. Electrochem. Soc.*, **158**, A498 (2011).

87. L. Chen, K. Wang, X. Xie and J. Xie, *J. Power Sources*, **174**, 538 (2007).

88. H. Ota, Y. Sakata, A. Inoue and S. Yamaguchi, *J. Electrochem. Soc.*, **151**, A1659 (2004).

89. O. Matsuoka, A. Hiwara, T. Omi, M. Toriida, T. Hayashi, C. Tanaka, Y. Saito, T. Ishida, H. Tan, S. S. Ono and S. Yamamoto, *J. Power Sources*, **108**, 128 (2002).

90. S. S. Zhang, *J. Power Sources*, **162**, 1379 (2006).

91. F. Ding, W. Xu, X. Chen, J. Zhang, M. H. Engelhard, Y. Zhang, B. R. Johnson, J. V. Crum, T. A. Blake, X. Liu and J.-G. Zhang, *J. Electrochem. Soc.*, **160**, A1894 (2013).

92. C. Jung, *Solid State Ionics*, **179**, 1717 (2008).

93. D. Aurbach, M. Moshkovich, Y. Cohen and A. Schechter, *Langmuir*, **15**, 2947 (1999).

94. S. Sylla, J. Y. Sanchez and M. Armand, *Electrochim. Acta*, **37**, 1699 (1992).

95. T. Kawamura, S. Okada and J.-i. Yamaki, *J. Power Sources*, **156**, 547 (2006).

96. B. Ravdel, K. M. Abraham, R. Gitzendanner, J. DiCarlo, B. Lucht and C. Campion, *J. Power Sources*, **119-121**, 805 (2003).

97. D. Aurbach, A. Zaban, Y. Ein-Eli, I. Weissman, O. Chusid, B. Markovsky, M. Levi, E. Levi, A. Schechter and E. Granot, *J. Power Sources*, **68**, 91 (1997).

98. S. Leroy, F. Blanchard, R. Dedryvère, H. Martinez, B. Carré, D. Lemordant and D. Gonbeau, *Surf. Interface Anal.*, **37**, 773 (2005).

99. A. Du Pasquier, F. Disma, T. Bowmer, A. S. Gozdz, G. Amatucci and J.-M. Tarascon, *J. Electrochem. Soc.*, **145**, 472 (1998).

요약 (국문초록)

흑연은 현재 리튬 이온 이차 전지에서 가장 많이 사용되는 음극 물질로, 0.3 V (*vs.* Li/Li^+) 이하에서 리튬 이온의 삽입/탈리 반응을 통해 용량을 발현한다. 이러한 흑연의 낮은 반응 전압으로 인해 전해질의 환원 분해는 불가피하다. 왜냐하면 현재 사용되는 유기 전해질의 전기화학적 산화/환원 전위창이 흑연 전극의 반응 전압 보다 높게 형성되기 때문이다. 전해질의 환원 분해는 흑연 전극 표면에 부동태막 (solid electrolyte interphase, SEI)을 형성하는데, 이러한 SEI 피막은 추가적인 전해질의 분해 반응을 억제하여 전지가 안정적으로 작동할 수 있도록 도와준다. SEI 피막은 전지의 성능 특성에 직접적인 영향을 줄 수 있기 때문에 기계적인 강도, 열적 안정성, 전극과의 접착성, 불용해성 등의 필수적인 요소들을 만족해야 한다. 그 중에서 피막의 열적 안정성은 전지의 수명 특성이나 보관 특성, 특히 안전성에 결정적인 영향을 미친다. 본 연구에서는 SEI의 피막의 열적 거동에 대해 분석하고 전기화학적 특성에 미치는 영향에 대해 알아보았다.

흑연 전극에서 기준 전해질 (1.0 *M* $LiPF_6$ in EC/DEC, (1:1, *vol.*))에 의해 형성된 SEI 피막의 열적 안정성을 평가하기 위해 OCV (open-circuit voltage) 측정 분석법을 수행하였다. 25도에서 120도까지 온도를 상승시키면서 셀의 OCV를 측정한 결과, 60도부터 OCV 값이 점점 증가하는 거동을 보이면서

결국 3.0 V까지 상승한다. 이는 셀이 고온에 노출됨에 따라 표면 피막이 손상되어 표면 보호 능력 (passivating ability)를 상실하기 때문이다. 표면 피막이 열적으로 불안정한 온도인 85도로 고정하여 고온 보관 실험을 진행하면, 단시간에 OCV 값이 3.0 V까지 상승하였다. 이러한 피막의 열적 안정성은 추후 상온에서의 전기화학적 성능에 영향을 미칠 수 있다는 것을 확인하였다.

고온에 노출된 표면 피막의 열적 거동을 분석하고 그에 따른 전기화학적 성능을 평가하기 위해, SOC (state-of-charge)를 각각 다르게 충전한 흑연 전극을 이용하여 분석하였다. 낮은 SOC의 전극에서는 고온 보관 시간이 길어질수록 표면 피막의 열적 손상이 심각하였다. 피막의 표면은 점점 거칠어지고, 피막 성분은 리튬염의 열분해 산물로 구성되고 원래 구성 물질들이 열에 의해 변형되었다. 또한 전극의 표면이 점점 노출되었는데, 이에 따라 고온 보관 후 상온에서 다시 정전류 충방전을 수행했을 시 큰 비가역 용량을 발생하며 낮은 쿨롱 효율 특성을 보였다. 한편, 높은 SOC의 전극에서는 피막이 열적으로 불안정한 85도에 노출되었음에도 불구하고 여전히 SEI로써 역할을 수행하였다. 즉, 피막의 표면 보호 능력 (passivating ability)으로 인해 낮은 SOC의 전극에서와는 상반되게 고온 보관 후에도 높은 쿨롱 효율 특성을 나타냈다. 높은 SOC의 전극은 충분히 많은 양의 전자를 가지고 있기 때문에 고온 보관 시 열적으로 손상된 표면 피막을 EC

전해질 환원 반응을 통해 재구축할 수 있었다. 재구축된 표면 피막은 최초의 SEI와 비교하여 표면 형상과 화학적 조성이 유사한 특징을 보였다.

마지막으로, 전해질의 리튬염에 따른 표면 피막의 열적 안정성 차이를 살펴보기 위해 비교군으로 LiTFSI (lithium bis(trifluoromethylsulfonyl)imide)가 녹아있는 전해질을 이용하여 $LiPF_6$ 가 녹아있는 기준 전해질과 비교 실험을 수행하였다. LiTFSI 가 녹아있는 전해질에 의해 생성된 표면 피막의 열적 안정성은 기준 전해질에 의해 생성된 피막보다 우수하였다. 85 도 고온에서 보관 시 OCV 변화는 작았고, 추후 상온에서 다시 정전류 충방전을 수행했을 시에도 상대적으로 높은 쿨롱 효율 특성을 보였다. 이러한 피막의 우수한 열적 안정성은 초기에 생성된 SEI 피막의 형태와 조성에 크게 의존하는 것으로 밝혀졌다. 많은 양의 유기물을 함유하는 표면 피막이 흑연 음극 위에 균일하게 덮여 있었기 때문에, 셀이 고온에 노출되어도 표면 피막은 여전히 표면 보호 능력 (passivating ability)를 유지할 수 있었다.

키워드: 리튬 이차 전지, 흑연, 표면 피막(SEI), 열적 안정성, 표면 보호 능력

학번: 2008-21080